



Journal of Energy Trends

Official journal of Atatürk University, Faculty of Engineering

Volume 1 • Issue 1 • June 2024

<https://dergipark.org.tr/en/pub/jet>

Journal of Energy Trends

CHIEF EDITOR

Faruk YEŞİLDAL 

Department of Mechanical Engineering,
Atatürk University, Erzurum, Türkiye

ASSOCIATE EDITORS

Nesrin ADIGÜZEL 

Department of Mechanical Engineering,
Atatürk University, Erzurum, Türkiye

Şükran EFE 

Department of Mechanical Engineering,
Atatürk University, Erzurum, Türkiye

LANGUAGE EDITOR

M.Kaan YEŞİLYURT 

Department of Mechanical Engineering,
Atatürk University, Erzurum, Türkiye

EDITORIAL BOARD

Davannendran CHANDRAN 

Department of Mechanical Engineering, Universiti Teknologi PETRONAS, Malaysia

Drilon MEHA 

Faculty of Mechanical Engineering, University of Prishtina, Kosovo

Farhan Lafta RASHID 

Department of Mechanical Engineering, University of Kerbala, Iraq

Hadi Ghasemi ZAVARAGH 

Department of Mechanical Engineering, Faculty of Al-khadir, Zanjan Branch, Technical and Vocational University (TVU), Tehran, Iran

Mohammad TAGHILOU 

Department of Mechanical Engineering, University of Zanjan, Zanjan, Iran

Raya AL-DADAH 

Department of Mechanical Engineering, University of Birmingham, UK

Aslıhan KURNUÇ SEYHAN 


Department of Mechanical Engineering, University of Erzincan Binali Yıldırım, Erzincan, Türkiye

Cihan YILDIRIM 

Department of Machinery and Metal Technologies, Ağrı İbrahim Çeçen University, Ağrı, Türkiye

Kenan YAKUT 

Department of Mechanical Engineering, Atatürk University, Erzurum, Türkiye

Mustafa İLBAŞ 

Department of Mechanical Engineering, Gazi University, Ankara, Türkiye

Sebahattin ÜNALAN 

Department of Mechanical Engineering, Erciyes University, Kayseri, Türkiye

Şaban PUSAT 

Department of Mechanical Engineering, Yıldız Technical University, İstanbul, Türkiye

Ünal AKDAĞ 

Department of Mechanical Engineering, Aksaray University, Aksaray, Türkiye

Yusuf Ali KARA 

Department of Mechanical Engineering, Bursa Technical University, Bursa, Türkiye



Journal of Energy Trends

REVIEWER BOARD

Abdüssamed KABAKUŞ ^{ID}

Department of Machine, Artvin Çoruh University, Artvin, Türkiye

Alptekin TÜRKKAN ^{ID}

Department of Electronics and Automation, Bursa Uludağ University, Bursa, Türkiye

Altuğ KARABEY ^{ID}

Department of Mechanical Engineering, Van Yüzüncü Yıl University, Van, Türkiye

Emre MANDEV ^{ID}

Department of Mechanical Engineering, Erzurum Technical University, Erzurum, Türkiye

Fevzi Çakmak BOLAT ^{ID}

Department of Mechanical Engineering, Kocaeli University, Kocaeli, Türkiye

Gürşah GÜRÜF ^{ID}

Department of Mechanical Engineering, Karabük University, Karabük, Türkiye

Halil İbrahim AKOLAŞ ^{ID}

Department of Motor Vehicles and Transportation Technologies, Balıkesir University, Balıkesir, Türkiye

Rahim Aytuğ ÖZER ^{ID}

Department of Mechanical Engineering, Kafkas University, Kars, Türkiye

Recep ÇATAR ^{ID}

Department of Mechanical Engineering, Bayburt University, Bayburt, Türkiye

Rıdvan YAKUT ^{ID}

Department of Mechanical Engineering, Kafkas University, Kars, Türkiye



Journal of Energy Trends

AIMS AND SCOPE

The journal focuses on critical aspects of energy, including energy sources, flow dynamics, internal combustion engines, battery technology, production systems, and consumption patterns. By disseminating this vital knowledge, we aim to foster collaboration between researchers, educators, and policymakers. The Journal of Energy Trends serves as a valuable resource for researchers actively engaged in or seeking to explore the vast field of mechanical engineering.

Disclaimer

Statements or opinions expressed in the manuscripts published in the journal reflect the views of the author(s) and not the opinions of the editors, editorial board, and/or publisher; the editors, editorial board, and publisher disclaim any responsibility or liability for such materials. When using previously published content, including figures, tables, or any other material in both print and electronic formats, authors must obtain permission from the copyright holder. Legal, financial and criminal liabilities in this regard belong to the author(s).

Open Access Statement

Journal of Energy Trends is an open access publication. Starting on 2024, all content published in the journal is licensed under the Creative Commons Attribution-NonCommercial (CC BY-NC) 4.0 International License which allows third parties to use the content for non-commercial purposes as long as they give credit to the original work. This license allows for the content to be shared and adapted for non-commercial purposes, promoting the dissemination and use of the research published in the journal. All published content is available online, free of charge at <https://dergipark.org.tr/en/pub/jet>



Contact (Editor in Chief)

Faruk YEŞİLDAL

Atatürk University, Department of
Mechanical Engineering, Erzurum, Türkiye



fyesildal@atauni.edu.tr



jet@atauni.edu.tr



<https://dergipark.org.tr/en/pub/jet>



+90 442 231 45 44

Contact (Publisher)

Atatürk University, Erzurum, Türkiye

Atatürk University, Erzurum, Türkiye



ataunijournals@atauni.edu.tr



<https://bilimseldergiler.atauni.edu.tr>



+90 442 231 15 16



Journal of Energy Trends

CONTENTS

Research Articles

- 1** *Experimental Investigation of Photovoltaic Systems Cooling with Binary Mixture Spray*
Furkan EGE, Kenan YAKUT
- 10** *Comparative Analysis of the Effect of Replacing Central System Heating and Cooling with VRF Technology on Energy Efficiency*
Ömer Faruk KARABUĞA, Nesrin ADIGÜZEL
- 21** *Numerical Investigation of The Flow Structure on Ground Surface Mounted Square Prism*
Onur KÜÇÜKKURT, Cuma KARAKUŞ
- 33** *Climate and Energy Analysis for Erzurum*
Zeynel Abidin BABA, Gökhan ÖMEROĞLU
- 42** *Numerical Study of the Aerodynamic Behavior of 7.62 x 51 mm Bullet*
Osman YAZICI, Şendoğan KARAGÖZ, Orhan YILDIRIM, Ömer ÇOMAKLI





Experimental Investigation of Photovoltaic Systems Cooling with Binary Mixture Spray

Fotovoltaik Sistemlerin İkili Karışım Sprey ile Soğutulmasının Deneysel İncelenmesi

Furkan EGE



Atatürk University, Faculty of Engineering, Mechanical Engineering Erzurum, Türkiye .

Kenan YAKUT



Atatürk University, Faculty of Engineering, Mechanical Engineering Erzurum, Türkiye.

ABSTRACT

In this study, it is aimed at achieving more effective and faster cooling by using a binary mixture (water-ethanol) in the spray cooling of photovoltaic systems. The panel cell temperature-efficient working range of photovoltaic systems can be defined as 25-45°C. In this experimental study, when the panel cell temperature exceeded 45°C at 1000 Wm⁻² radiation, spray cooling was performed until it was reduced to 25°C. In the cooling process, faster cooling was achieved by using 15%, 30% and 45% ethanol in the binary mixture. The DXD-HSI-6 nozzle was used at different liquid and air flow rates in the spray cooling experiment setup, and the ALR (air-liquid ratio) was calculated. In the spray cooling process of the photovoltaic system with a binary mixture, the effect of ethanol on cooling was investigated in all experiments. The fastest cooling was achieved at a liquid flow rate of 800 ml/min and an air flow of 4.5 m³/h. In the cooling process with pure water, it has been observed that the panel cell temperature can be reduced below 25°C by applying a 100-second spray, and when 45% ethanol is added, the time is reduced to 75 seconds by cooling 25% faster.

Keywords: Spray cooling, atomization, Photovoltaic system, binary mixture, ethanol.

Öz

Bu çalışmada, fotovoltaik sistemlerin sprey soğutmasında ikili karışım (su-etanol) kullanılarak daha etkili ve hızlı soğutma sağlanması amaçlanmıştır. Fotovoltaik sistemlerin panel hücre sıcaklığı verimli çalışma aralığı 25-45°C olarak tanımlanabilir. Bu deneysel çalışmada, panel hücre sıcaklığı 1000 Wm⁻² radyasyonda 45°C'yi aştığında, 25°C'ye düşene kadar sprey soğutma uygulanmıştır. Soğutma sürecinde, ikili karışım da %15, %30 ve %45 etanol kullanılarak daha hızlı soğutma sağlanmıştır. Sprey soğutma deney düzeninde farklı sıvı ve hava akış hızlarında DXD-HSI-6 meme kullanılmış ve ALR (hava-sıvı oranı) hesaplanmıştır. İkili karışım ile fotovoltaik sistemin sprey soğutma sürecinde, tüm deneylerde etanolün soğutma üzerindeki etkisi araştırılmıştır. En hızlı soğutma, 800 mldak⁻¹ sıvı akış hızı ve 4.5 m³sa⁻¹ hava akışı ile elde edilmiştir. Saf su ile soğutma sürecinde, panel hücre sıcaklığının 100 saniyelik sprey uygulaması ile 25°C'nin altına indirilebileceği ve %45 etanol eklendiğinde, sürenin %25 daha hızlı soğutma ile 75 saniyeye düştüğü gözlemlenmiştir.

Anahtar kelimeler: Püskürtmeli soğutma, atomizasyon, Fotovoltaik sistem, ikili karışım, etanol.



Received/Geliş Tarihi : 23.05.2024
Accepted/Kabul Tarihi : 13.06.2024
Publication Date/Yayın Tarihi : 30.06.2024

Corresponding Author/Sorumlu Yazar:
Furkan EGE
E-mail: furege17@gmail.com

Cite this article: Ege F., Yakut K., (2024).
Experimental Investigation of Photovoltaic
Systems Cooling with Binary Mixture Spray.
Journal of Energy Trends, 1(1), 1-9



Content of this journal is licensed under a
Creative Commons Attribution-Noncommercial
4.0 International License.

Introduction

Nowadays, the majority of the energy needed is obtained from fossil fuel sources. It causes water, soil, and air pollution in the environment due to the harmful waste produced as a result of the processing of fossil fuels. In addition, fossil fuels have disadvantages such as being limited and not sufficient to meet the ever-increasing energy need. For this reason, instead of fossil fuels, which cause negativities such as climate change and environmental pollution on a global scale, it has necessitated the use of renewable energy sources, which are of great importance for the future of living things, and cause less destruction in the environment and active use of energy (Anonymous 2018). One of the most important advantages of renewable energy sources is that they help protect the environment by reducing harmful gas emissions. Another important advantage is that they contribute to increasing employment in energy and reducing dependence on foreign countries, as they are domestic resources (Akman, 2019).

Solar energy, one of the renewable energy sources, has the feature of having an endless energy source and is used today in heating workplaces and homes, using hot water and producing electricity (Özgeçmen, 2007). All of the solar radiation absorbed by photovoltaic layers cannot be converted into electrical energy, and some of it is given to the environment as waste heat. Waste heat given to the environment causes the electric current efficiency of the solar layer to decrease, which causes the temperature value of the solar panels to increase (Huang et al., 2001). The output power of photovoltaic cells decreases when the operating temperatures of solar panels increase. For this reason, it is important to maintain the optimal operating temperature of solar cells in order to have better performance (Akman, 2019). Photovoltaic thermal systems (PV/T) (Figure 1), which are among the solar systems, are systems that cool the waste heat generated by solar energy that cannot be converted into electrical energy, remove it from the cell, and convert it into a useful position by keeping the operating temperature of the system at the same level.

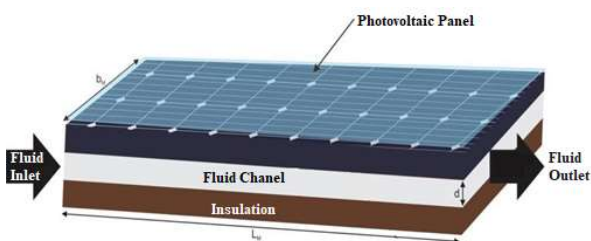


Figure 1.
A General PV/T System Schematic (Diwaniq, 2020).

In 1976, Martin Wolf first mentioned the combination of the photovoltaic system and the liquid heating thermal method using the Hottel-Whillier analysis method on a flat plate. As a result of this analysis, it has been revealed that PV/T systems are feasible in terms of cost and technique, and that the energy production in the reduced surface area is quite high by minimizing the installation usage area compared to classical thermal methods. Anonymous (2020) Microchips, one of the most advanced technologies with high power, need to remove a large amount of heat from a limited surface. In order to solve such problems, it is of vital importance that the heat fluxes of microchip components in computers be 500 Wcm^{-2} and their hot points be 1000 Wcm^{-2} in the coming years. Such high requirements can be met by direct cooling methods such as spray cooling (Figure 2).

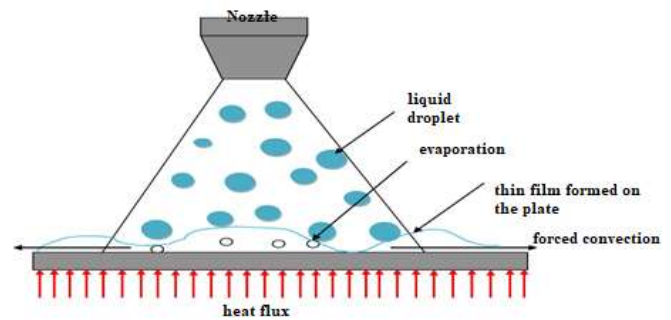


Figure 2.
Spray Cooling (Jafari, 2014).

The physical properties of alcohol make it an ideal additive in the practical application of electronic cooling due to its environmental friendliness and good compatibility with other materials, and it is soluble. No device or nozzle corrosion due to salts or clogging by nanoparticles. It has been shown that adding a small amount of alcohol to water can significantly reduce the surface tension and contact angle. It is an effective way to increase heat dissipation and control surface temperature simultaneously. As the alcohol content increases, the heat transfer capacity enhancement intensity first increases and then weakens slightly. For spray atomization, the Weber number, which is the ratio of inertial forces to surface tension forces, must be high, and adding alcohol to water increases the Weber number (Liu et al., 2019).

$$We = \frac{\rho_l v^2 D_0}{\sigma} \quad (1)$$

Spray cooling

It is a cooling mechanism in which phase variation occurs with spray droplets to increase the efficiency of heat transfer. Spray

cooling is used in the cooling of hot gases, in the skin area, in the cooling of electronic devices where high temperatures are not preferred, and in fire protection (Figure 3). Spray cooling plays an important role in improving microstructures after steel strip casting and hot rolling with high temperature levels (up to 1800 K) from the operating industry and metal production. Characteristically, it is sprayed into hot areas to cool jet fuel carrying water droplets. The heat transfer mechanism in spray cooling is divided into 4 main groups. The list of them;

- Fixed nucleation surfaces in the heated area
- Convection forced by the impact of droplets,
- Evaporation on the film surface,
- It is secondary nucleation with spray droplet

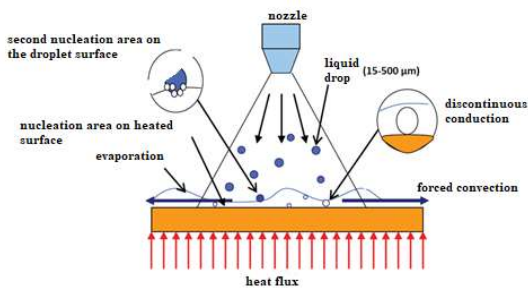


Figure 3.
Mechanism of heat transfer in spray (Yan et al. 2011).

Evaporation from liquid thin film layer

The evaporation of liquid molecules from the liquid layer area is an important heat transfer mechanism for cooling the spray. The schematic view of the formation of a liquid film on the heated area when spray cooling is started is given in Figure 4. This layer is generally 300-500 μm thin.

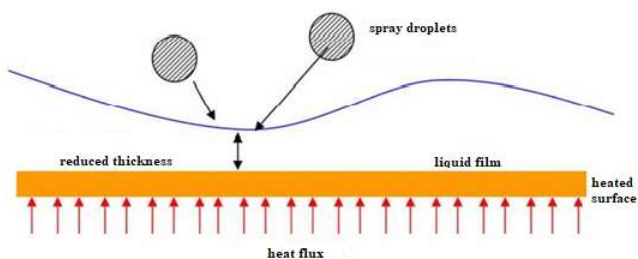


Figure 4.
View of evaporation from the liquid film layer (Yan et al. 2011).

Forced convection as a result of impact of droplets

As a result of the droplets hitting the thin liquid layer, the force generated by the droplets causes enhanced forced convection in the liquid layer (Figure 5). In forced convection, the fluid is forced to flow over a compressor, fan, pump, or similar surface or into the tube, depending on an external factor.

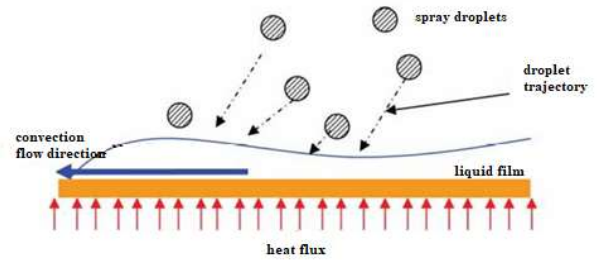


Figure 5.
Appearance of forced convection as a result of impact of droplets (Yan et al. 2011).

Fixed nucleation zones in the heated layer

When the studies on this subject are examined, it has been determined that bubbles grow in fixed nucleation areas on the heated surface. It has been reported that this is caused by growth-promoting activations in the bubbles. The bubbles begin to grow in the core area, absorbing heat from the heated region (Figure 6).

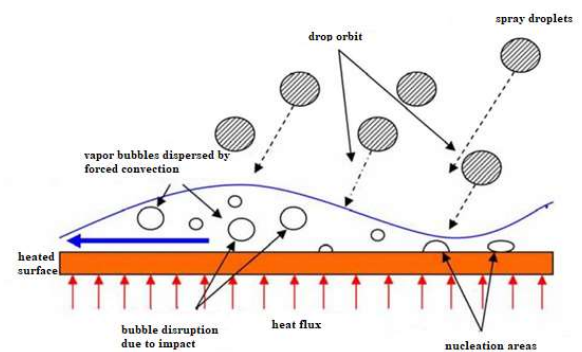


Figure 6.
View of the fixed nucleation zone in the heated area (Yan et al. 2011).

Due to the large number of secondary core regions due to spray droplets, spray cooling is an important mechanism for removing the high heat flux coming from the surface heated by the boiling of the pool. (Yan et al. 2011)

Spray cooling is an effective cooling method for high heat flux applications due to its high heat removal capacity at low coolant flow rates. In spray cooling, coolant droplets produced by the spray nozzle continuously impinge on a hot surface and remove heat through forced convection, thin-film evaporation, or even nuclei boiling. Over the past few decades, a number of studies have focused on the spray nozzle, coolant, spray characteristics, cooling regimes, and surface treatment. It has been studied experimentally using water sprays produced by a full-cone nozzle to cool a sputter-coated thin-film heater on a silicon wafer. For best cooling, the optimum spray height occupies less space than the heater, and the optimum spray height decreases

with increasing flow rate. It was found that the increase and decrease of cooling performance is generally consistent with the increase and decrease of spray flow (Gao and Li, 2017).

In this study, where the atomization effects on the heat transfer properties of spray cooling are explained, it has been seen that the heat transfer effect can be improved as the diameter of the nozzle increases. The results of the spray coating width were seen at 20 Lh^{-1} and 30 Lh^{-1} flow rates. It sprayed 30 mm at 20 Lh^{-1} and 40 mm at 30 Lh^{-1} . The angle of the spray cone has significant effects on cooling. As the diameter of the nozzle increases, the exit velocity of the droplet and the angle of the spray spine decrease, and the heat transfer effect can be improved (Bao et al., 2019).

In the study by Nategi et al. (2021) spray cooling was experimentally examined to increase photovoltaic panel efficiency. In this experiment, the effects of spray angle, distance of the nozzles to the PV panel, number of nozzles and vibrating water spray on the PV panel performance were investigated. Spray angles varied from 15° to 50° . It was shown that decreasing the spray angle by 15° increased the electrical efficiency of the PV panel to 19.78% and simultaneously decreased the average PV temperature from 64° to 24° . Additionally, the nozzle-to-PV panel distance was changed from 10 cm to 50 cm, and the best result was achieved for the lowest distance, with an 86% increase in power output. The effects of water spray angle, water flow rate, and nozzles on PV panel distance were evaluated for PV panel performance. Experiments show that water spray cooling improves PV panel performance. The results of this study support the idea that electrical efficiency and output power increase by reducing the spray angle of the cooling water.

Wibowo et al. (2024), This research investigates the cooling effects of different types and sizes of water sprays on photovoltaic (PV) panels to enhance performance by reducing temperature. Conducted between 08:00-15:00, it was found that a full cone nozzle with a 2 mm diameter reduced panel temperature from 61.96°C to 36.51°C and increased efficiency from 10.98% to 14.47%. Full cone nozzles provided better cooling due to more even water distribution compared to hollow cone and flat fan nozzles. Variations in nozzle diameter also impacted cooling effectiveness.

In the study conducted by Kim et al. (2007) a steel plate was heated to 900°C in a muffle furnace. Coolants were also prepared at room temperature ($25^\circ\text{C} \pm 1^\circ\text{C}$). The nozzle currently used is a full-cone spray nozzle. In the study, (0, 100, 300, 500, 700) ppm ethanol concentration and then 56 ppm surfactant (tween 20) refrigerant were used (Figure 8). The results show that the contact angle value decreases with

increasing ethanol concentrations in water. Various coolers have different cooling capacities, which can be defined in terms of coolant consumption and cooling time. The lower the cooling time spent by a cooler, the lower the consumption and, therefore, the higher the cooling capacity. It has been observed that this can be achieved by decreasing the contact angle of the water droplet with the solid surface and increasing the concentration of surfactant or alcohol in the water droplets to ensure rapid evaporation. Additionally, the improvement of spray cooling with an ethanol-water mixture was observed (Figure 7 a,b). In this study, where the results of the nozzle height were also seen, it was seen that the 40 mm distance was more optimized in the experiments conducted between the (20-100) mm plate and the nozzle and gave better results in this and other studies. The surface tension and contact angle of pure ethanol are very low compared to pure water. Therefore, when ethanol is added to water, the contact angle of the resulting droplet decreases as the ethanol concentration increases (Figure 7) (Table 1).

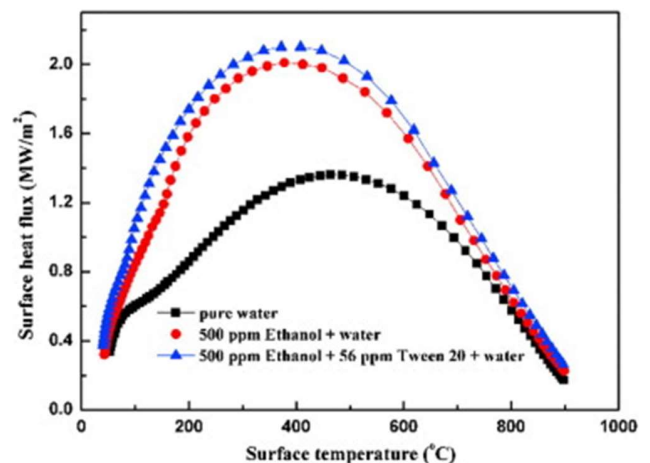


Figure 7.a.
Boiling curve for surfactant (tween 20)-ethanol-water mixture (Bhatt NH et al. 2017).

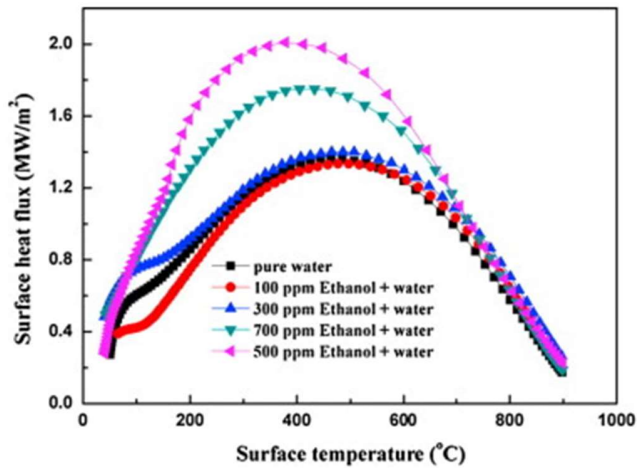


Figure 7.b.
Boiling curve for ethanol-water mixture (Bhatt NH et al. 2017).

Table 1.
A Table of Velocities (Bhatt NH et al. 2017).

Coolant	Cooling Rate ($^{\circ}\text{C}\text{s}^{-1}$)
Pure water	45
Ethanol 100ppm	57
Ethanol 300ppm	61
Ethanol 500ppm	70
Ethanol 700ppm	55

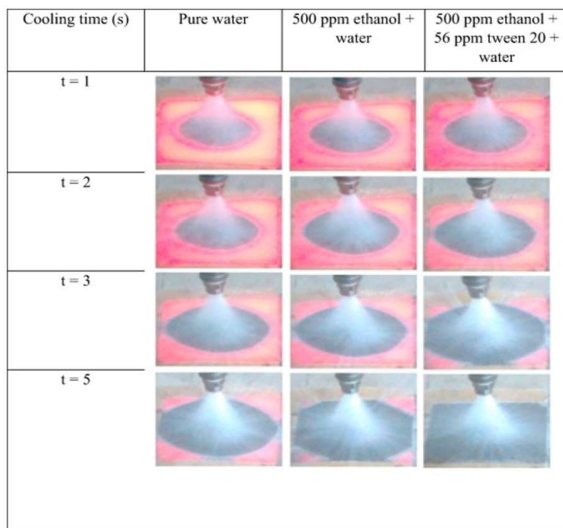


Figure 8.
Water, 500ppm ethanol + water, 500ppm ethanol + 56 ppm tween 20 + water cooling phases in 5 seconds were recorded (Bhatt NH et al. 2017).

An experimental study presents the optimization of the parameters involved in air-assisted water spraying on the PV panel surface. The effect of spray cooling on panel performance was examined and electrical efficiency decreased due to the increase in cell temperature. Effective parameters have been determined to prevent this decline. These parameters were

examined at three levels: spraying time, spraying flow rate, nozzle air flow rate, nozzle-to-panel distance, and solar radiation. As a result, the optimum values for the highest electrical efficiency were obtained as 49.9 s for spraying time, $0.0180 \text{ m}^3\text{hour}^{-1}$ for spraying flow rate, $2 \text{ m}^3\text{hour}^{-1}$ for air flow rate, 50 cm and 700 Wm^{-2} for the distance from nozzle to panel (Yesildal, F. et al. 2021).

In this experimental study, the system was designed by taking into account other studies in the literature, and by using ethanol + water in different ratios with controlled spray cooling and by trying the DXD-HSI-6 nozzle type to reduce the temperature increase caused by solar radiation coming directly to the cells of the Photovoltaic system. Cooling formation was observed. Additionally, it has been observed that using 15% (15-30-45%) ethanol provides better cooling than water.

Material and Methods

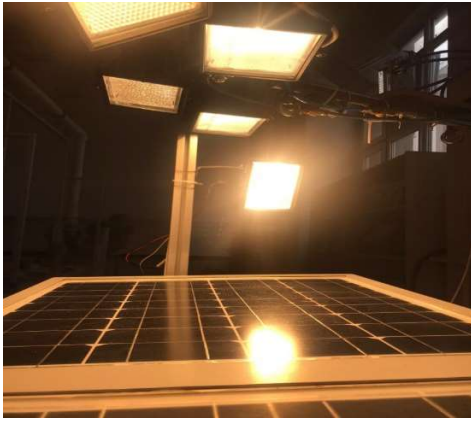
Experimental setup

A nozzle, positioned at a height where the spray can form, and five halogen lamps, each with a power of 500 W, have been placed on the photovoltaic panel. The nozzle, which has air and water inlets, is set to supply pressurized air from an air tank pressurized by a compressor up to a maximum of 8 bars, and water + ethanol and water from a 20-liter water tank pressurized up to a maximum of 4 bars. After making the necessary adjustments, a maximum air flow of $4.5 \text{ m}^3\text{h}^{-1}$ and a minimum air flow of $3 \text{ m}^3\text{h}^{-1}$ were provided in the air flow meters. In the water flow meter, a minimum liquid flow of 400 mlmin^{-1} and a maximum liquid flow of 800 mlmin^{-1} were provided. These minimum and maximum values were adjusted according to the atomization of the spray.

The system operates within the temperature range of $25\text{-}45^{\circ}\text{C}$, and the start and end times of the spray are recorded with the help of a data logger based on these temperatures. The spray cooling starts at 45°C and continues until the temperature drops to 25°C . (Figure 9-10) (Table 3). Here D_0 represents the diameter of the nozzle and σ_1 represents the surface tension. The physical properties of ethanol are given in Table 2.

Table 2.*Physical Properties of Ethanol at 25°C (Xu H. et al. 2021).*

Property	Unit	Value
Intensity	kgm ⁻³	789
Surface tension	Nm ⁻¹	21.97 × 10 ⁻³
Dynamic viscosity	mPa.s	1.074
Electrical conductivity	Sm ⁻¹	5 × 10 ⁻⁵
Boiling point	°C	78
Specific heat	kJ(kg°C) ⁻¹	2.58
Heat of vaporization	kJkg ⁻¹	837.36
Thermal conductivity	W(mK) ⁻¹	0.171

**Figure 9.***General View of the Experimental Setup***Table 3.***Materials Used in the Experiment System*

1	Halogen Projector	9	Water tank
2	Variac	10	Heat and Air Inlet Pressure
3	Pyranometer	11	Water and Air Flowmeter
4	Photovoltaic Panel	12	Nozzle
5	Data Recorder	13	CCD Camera
6	Power Analyzer	14	Theme Camera
7	Compressor	15	Computer
8	Air tank	T 1-6	Thermocouples

DXD-HSI-6 nozzles, which have a single piece spraying feature, are atomized after air-water entry. Nozzles with a full cone spray amount have a maximum coverage area of 35 cm.

Table 4.*DXD-HSI 6 Technical Specifications*

MODEL	DXD-HSI-6
Liquid and air inlet	¼" BSB
Hole diameter at liquid inlet	Ø4 mm
Nozzle hole diameter	Ø1 mm

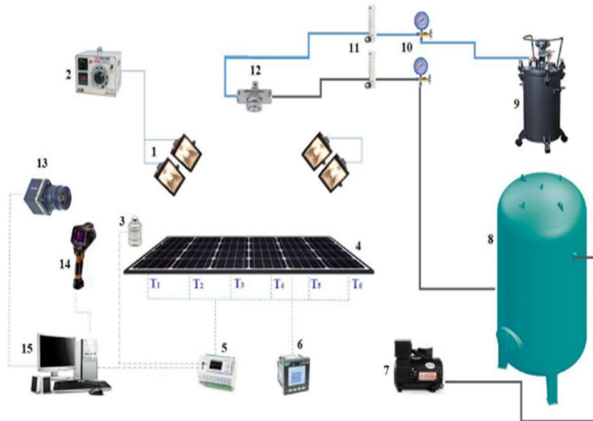
Results

Experimental data of pure water and ethanol mixtures

The experimental results of 3 m³h⁻¹ and 4.5 m³h⁻¹ air flow rates and 400 mlmin⁻¹ and 800 mlmin⁻¹ pure water and ethanol mixtures in certain proportions are detailed in the graphs below. are given, and ALR (air-liquid) ratios are calculated.

$$ALR = \frac{m_{air}}{m_{liq}} \quad (2)$$

In the spray cooling experiment performed by adding only water and 15%, 30% and 45% ethanol to water at an air flow rate of 3 m³h⁻¹ and a liquid flow rate of 400 mlmin⁻¹, when only water was used, the panel temperature changed from 45°C to 25°C in 120 seconds. It has also been observed that it cools. It was observed that faster cooling compared to water was achieved at rates of 32.52% in the 15% ethanol mixture, 41.8% in the 30% ethanol mixture, and 44.1% in the 45% ethanol mixture (Figure 11).

**Figure 10.***Experimental system schematic representation*

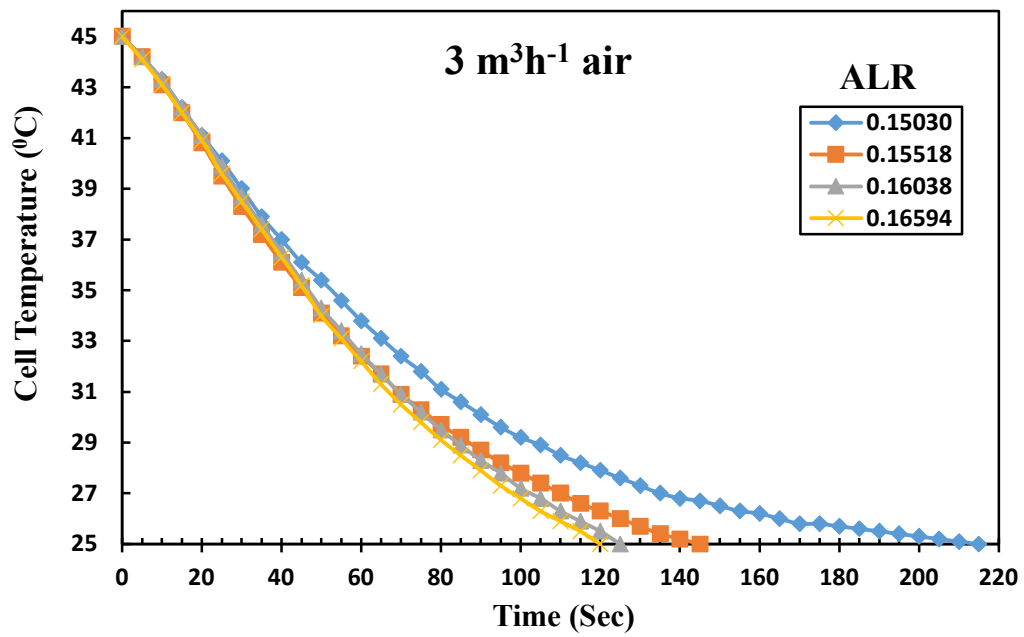


Figure 11.

Time-dependent cooling chart at 3 m³h⁻¹ air and 400 mlmin⁻¹ liquid

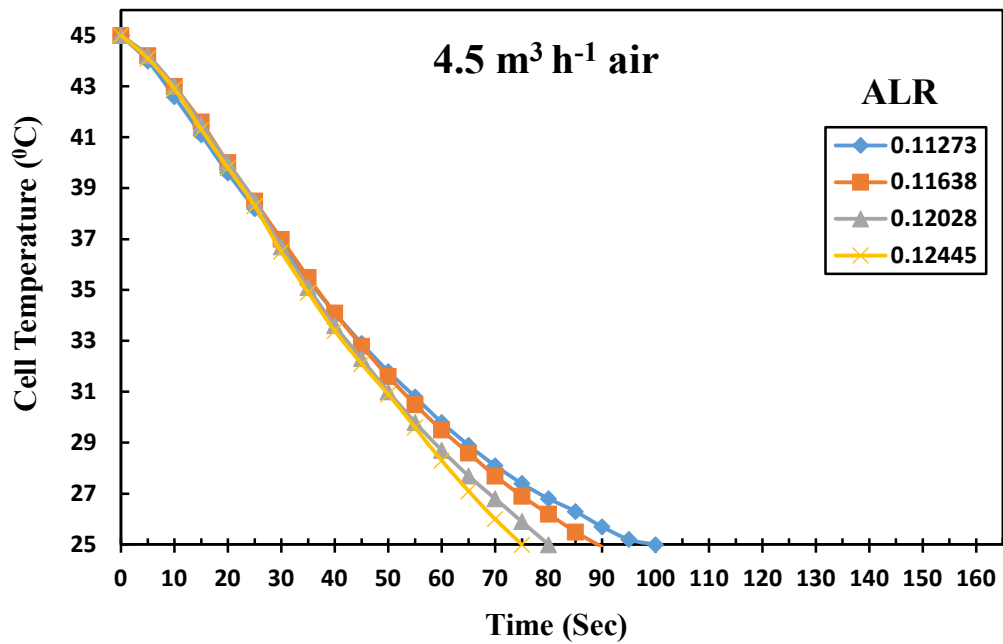


Figure 12.

Time-dependent cooling chart in 4.5 m³h⁻¹ air and 800 ml.min⁻¹ liquid

Table 5.
Fluid and ALR Ratios

Fluid	ALR
Water	0.15030
Water + % 15 ethanol	0.15518
Water + % 30 ethanol	0.16038
Water + % 45 ethanol	0.16594

In the spray cooling experiment performed by adding only water and 15%, 30% and 45% ethanol to the water at an air flow rate of $4.5 \text{ m}^3\text{h}^{-1}$ and a liquid flow rate of 800 mlmin^{-1} , the panel temperature increased from 45°C to 25°C by 100°C when only water was used. It has been observed that it cools in seconds. It was observed that when ethanol was added at the specified rates, faster cooling was achieved with a decrease of 10-20-25% respectively (Figure 12).

$$W_R = \frac{\partial w_r}{\partial x} = \left[\left(\left(\frac{\partial R}{\partial x_1} \right) w_1 \right)^2 + \left(\left(\frac{\partial R}{\partial x_2} \right) w_2 \right)^2 + \left(\left(\frac{\partial R}{\partial x_3} \right) w_3 \right)^2 + \dots + \left(\left(\frac{\partial R}{\partial x_n} \right) w_n \right)^2 \right] \quad (3)$$

Here, R is the function of the independent variables. The uncertainty of the independent variables is named w_1, w_2, w_n . $W_R(x_1, x_2, \dots, x_n)$ is the amount of uncertainty consisting of different independent variables (Table 16)

Table 7.
Uncertainties Measured in Parameters

Variable	Uncertainty (WR)
Air Flow Rate	0.08
Water Flow Rate	0.055
Heat	0.0143
Nozzle Diameter	0.001
Pressure	0.045
Pyranometer	0.027

Conclusions

In this study, the solar radiation intensity of photovoltaic panel systems cooled by binary mixture spray the decrease in cooling rate compared to water by mixing ethanol in certain proportions were examined. Optimum operating temperature ranges, air-liquid flow rates, and ethanol ratios were determined for the

Table 6.
Fluid and ALR Ratios

FLUID	ALR
Water	0.11273
Water + % 15 ethanol	0.11638
Water + % 30 ethanol	0.12028
Water + % 45 ethanol	0.12445

Uncertainty analysis

In the spray cooling process in the photovoltaic panel system, measurements were made with temperature, flow, and pressure measurement elements. Uncertainty analyses for the measurements were made. Uncertainty analyses provide reliable information about the experimental results obtained. The most important effect of these analyses is to determine the one that causes the highest deviation among the parameters in the experiments (Akpınar, 2005). Deviations that occur in the measurement of test inputs can be grouped as random, fixed, and production-related deviations. The equation given below was used to calculate the total error (Holman, 2012).

experiments, and the results obtained at the end of the experiments are given below.

In the spray cooling experiment conducted at 1000 Wm^{-2} radiation, it was observed that the effect of ethanol on cooling was positively reflected and the decrease in the cooling rate was directly proportional to the increase in ethanol.

The refrigerant we used in the binary mixture spray cooling experiments is ethanol. Due to the thermodynamic properties of ethanol, whose boiling point temperature is lower than that of water, ethanol mixed in certain proportions has an effect on cooling.

In spray cooling performed with 15%, 30% and 45% ethanol mixtures, it has been observed that as the ratio of ethanol increases, the effect of spray cooling increases compared to water.

According to the calculated ALR ratios, it has been observed that as the ALR ratios increase, the cooling times decrease.

The fastest cooling time for water was found to be 100 seconds in the spray cooling process at $4.5 \text{ m}^3\text{h}^{-1}$ air and an 800 mlmin^{-1} liquid flow rate.

The longest cooling time for water was 230 seconds in the spray cooling process at $3 \text{ m}^3\text{h}^{-1}$ air and a 400 mlmin^{-1} liquid flow rate.

It has been observed that cooling performance increases as the ethanol ratio increases. This increase is due to the fact that ethanol provides a more effective heat transfer mechanism due to its lower surface tension and higher evaporation capacity compared to water.

As a result, the binary mixture spray cooling method has been determined to be an effective method for cooling photovoltaic systems. The use of an ethanol-water mixture shortens the cooling time. These findings contribute to more efficient use of renewable energy resources and increased efficiency in energy production.

Peer-review: Externally peer-reviewed

Author contributions:

F.E.: Methodology, data curation, visualization, investigation and experimental analysis.

K.Y.: Supervision, original draft preparation.

Financial disclosure: This study was supported by Atatürk University Scientific Research Coordinatorship with Project Id of FBA-2021-9594.

Conflict of Interest: The author has no conflicts of interest to declare.

References

- Anonymous, 2018. Yenilenebilir enerjinin dalları ve açıklaması, <https://yenilenebilirenerjisistemi.blogspot.com/2018/02/enerji-si-yenilenebilir-enerjikaynaklar.html> (20.05.2020)
- Akman, Ö. (2019). Fotovoltaik Panellerde Sıcaklığın Elektriksel Verime Etkileri ve Termal Güç Eldesi. [Yüksek Lisans Tezi, Karabük Üniversitesi, Fen Bilimleri Enstitüsü, Karabük].
- Özgeçmen, A. (2007). Güneş Pilleri Kullanarak Elektrik Üretimi, [Yüksek Lisans Tezi, Gazi Üniversitesi Fen Bilimleri Enstitüsü, 112s, Ankara].
- Huang, S., Lin, T., Hung, W., & Sun, F. (2001). Performance Evaluation Of Solar Photovoltaic/Thermal Systems, *Solar Energy*, 70 (5), 443-448.
- Diwania, S., Agrawal, S., Siddiqui, A., S. & Singh, S. (2020). Photovoltaic–thermal (PV/T) technology: a comprehensive review on applications and its advancement. *International Journal of Energy and Environmental Engineering*, (11), 33–54.
- Anonymous, (2020). Performance of Photovoltaic Thermal Collector (PV/T) with Different Absorbers Design. <http://www.wseas.us/elibrary/transactions/environment/2009/31-968.pdf>.
- Jafari, M. (2014). Analysis of heat transfer in spray cooling system using simulations. [MS Thesis, Mechanical, Automotive and Materials Engineering, University of Windsor, Canada].
- Liu, H., Cai, C., Jia, M., Gao, J., Yin, H., & Chen, H. (2019). Experimental investigation on spray cooling with low-alcohol additives. *Applied Thermal Engineering*, 146, 921-930.
- Xu, H., Wang, J., Li, B., Yu, K., Tian, J., Wang, D., & Zhang, W. (2021). Effect of spray modes on electrospray cooling heat transfer of ethanol. *Applied Thermal Engineering*, 189, 116757.
- Yan, L., & Kim, I. H. (2011). Effect of dietary grape pomace fermented by *Saccharomyces boulardii* on the growth performance, nutrient digestibility and meat quality in finishing pigs. *Asian-Australasian Journal of Animal Sciences*, 24(12), 1763-1770.
- Gao, X., & Li, R. (2017). Effects of nozzle positioning on single-phase spray cooling. *International Journal of Heat and Mass Transfer*, 115, 1247-1257.
- Bao, J., Wang, Y., Xu, X., Niu, X., Liu, J., & Qiu, L. (2019). Analysis on the influences of atomization characteristics on heat transfer characteristics of spray cooling. *Sustainable Cities and Society*, 51, 101799.
- Nateqi, M., Rajabi Zargarabadi, M., & Rafee, R. (2021). Experimental investigations of spray flow rate and angle in enhancing the performance of PV panels by steady and pulsating water spray system. *SN Applied Sciences*, 3, 1-13.
- Santiko Wibowo, Z. A., Rachmanto, R. A., Himawanto, D. A., & Prasetyo, S. D. (2024). Optimization of Photovoltaic Performance Using a Water Spray Cooling System with Different Nozzle Types. *International Journal of Computational Methods and Experimental Measurements* 12(1), 9-19.
- Kim, J. (2007). Spray cooling heat transfer: The state of the art. *International Journal of Heat and Fluid Flow*, 28(4), 753-767.
- Bhatt, N. H., Raj, R., Varshney, P., Pati, A. R., Chouhan, D., Kumar, A., ... & Mohapatra, S. S. (2017). Enhancement of heat transfer rate of high mass flux spray cooling by ethanol-water and ethanol-tween20-water solution at very high initial surface temperature. *International Journal of Heat and Mass Transfer*, 110, 330-347.
- Yesildal, F., Ozakin, A. N., & Yakut, K. (2022). Optimization of operational parameters for a photovoltaic panel cooled by spray cooling. *Engineering Science and Technology, an International Journal*, 25, 100983.
- Akpınar, E. (2005). Deneysel çalışmalardaki hata analizinde bir örnek: Kurutma deneylerindeki hata analizi. *Mühendis ve Makina*, 46(540), 41-48.
- Holman, J. (2012). Experimental methods for engineers, 5th edition. McGraw-Hill, 739, New York, USA



Comparative Analysis of the Effect of Replacing Central System Heating and Cooling with VRF Technology on Energy Efficiency

Merkezi Sistem Isıtma ve Soğutmanın VRF Teknolojisi ile Değiştirilmesinin Enerji Verimliliği Üzerindeki Etkisinin Karşılaştırılmalı Analizi

Ömer Faruk KARABUĞA



Atatürk University, Institute of Science, Department of Mechanical Engineering, Erzurum, Türkiye .

Nesrin ADIGÜZEL



Atatürk University, Faculty of Engineering, Mechanical Engineering, Thermodynamics Department Erzurum, Türkiye.

ABSTRACT

In today's landscape, where energy efficiency and environmental impact are paramount in heating and cooling systems, Variable Refrigerant Flow (VRF) technology emerges as a compelling alternative to traditional systems. This article thoroughly evaluates the benefits of VRF technology, emphasizing its flexibility, efficiency, and cost-effectiveness.

VRF systems, with their dynamic refrigerant flow control, offer superior energy efficiency compared to fixed-speed traditional systems. This adaptability to varying heat demands enhances operational efficiency and reduces energy consumption, making VRF technology a sustainable choice.

Financial analysis further supports the case for VRF technology, demonstrating significant long-term cost savings. A case study of a student dormitory in Mersin illustrates the practical application of VRF, with detailed heat loss and gain calculations informing equipment selection.

Comparing selected Fan Coil Units (FCU) with VRF systems reveals a substantial 28% reduction in operating costs with VRF. Consequently, transitioning to VRF systems presents both economic and environmental advantages, as demonstrated by the successful implementation in the dormitory project.

In summary, this study highlights the transformative potential of VRF technology in improving energy efficiency, reducing costs, and enhancing sustainability in heating and cooling systems. Aimed at industry professionals and engineers, this analysis serves as a valuable guide in adopting more efficient and environmentally friendly solutions.

Keywords: VRF, Fan Coil, Conventional Water Systems, Energy Consumption.

ÖZ

Günümüzde enerji verimliliği ve çevresel etkinin ısıtma ve soğutma sistemlerinde ön planda olduğu bir dönemde, Değişken Soğutucu Akışkan Debisi (VRF) teknolojisi, geleneksel sistemlere kıyasla cazip bir alternatif olarak öne çıkmaktadır. Bu makale, VRF teknolojisinin esneklik, verimlilik ve maliyet etkinliği gibi faydalarını ayrıntılı bir şekilde değerlendirmektedir.

VRF sistemleri, dinamik soğutucu akışkan debi kontrolü ile sabit hızlı geleneksel sistemlere göre üstün enerji verimliliği sunar. Değişen ısı taleplerine uyum sağlama yeteneği, işletim verimliliğini artırır ve enerji tüketimini azaltır, bu da VRF teknolojisini sürdürülebilir bir seçenek haline getirir.

Mali analizler, VRF teknolojisinin uzun vadede önemli maliyet tasarrufları sağladığını göstermektedir. Mersin'deki bir öğrenci yurdu örneği, VRF'nin pratik uygulamasını, ısı kaybı ve kazancı hesaplamalarıyla detaylandırarak ekipman seçiminde nasıl bir yol izlendiğini ortaya koymaktadır.



Received/Geliş Tarihi : 22.03.2024
Accepted/Kabul Tarihi : 30.04.2024
Publication Date/Yayın Tarihi : 30.06.2024
Corresponding Author/Sorumlu Yazar:
Ömer Faruk KARABUĞA
E-mail: omerkara714@gmail.com

Cite this article: Karabuga, O.F; Adiguzel N., (2024). Comparative Analysis of the Effect of Replacing Central System Heating and Cooling with VRF Technology on Energy Efficiency. *Journal of Energy Trends*, 1(1), 10-20



Content of this journal is licensed under a Creative Commons Attribution-NonCommercial 4.0 International License.

Seçilen Fan Coil Üniteleri (FCU) ile VRF sistemlerinin karşılaştırılması, VRF ile işletme maliyetlerinde %28'lik önemli bir azalma olduğunu göstermektedir. Sonuç olarak, VRF sistemlerine geçiş hem ekonomik hem de çevresel avantajlar sunmakta, yurt projesindeki başarılı uygulama bunu kanıtlamaktadır.

Özetle, bu çalışma, VRF teknolojisinin enerji verimliliğini artırma, maliyetleri düşürme ve ısıtma ve soğutma sistemlerinde sürdürülebilirliği artırma konusundaki dönüştürücü potansiyelini vurgulamaktadır. Sektör profesyonelleri ve mühendisler için hazırlanan bu analiz, daha verimli ve çevre dostu çözümlerin benimsenmesi konusunda değerli bir rehber niteliğindedir.

Anahtar kelimeler: VRF, Fan Coil, Geleneksel Sulu Sistemler, Enerji Tüketimi

Introduction

The negative effects of fossil fuels (coal, oil, etc.) on human life and our planet continue. In this context, efforts are ongoing to increase energy efficiency and improve comfort parameters in devices and systems used for heating and cooling. Variable Refrigerant Flow (VRF) and Fan Coil Unit (FCU) applications stand out as systems reflecting these efforts. VRF systems, with their flexible architectural and geometric compatibility features, can be used in various structures, from schools to hospitals, providing energy-saving capabilities by performing heating and cooling processes.

FCU systems can be configured as 2-pipe or 4-pipe. While a 2-pipe system can only perform heating or cooling, a 4-pipe system can operate in both heating and cooling modes simultaneously, depending on user preferences and space requirements. System equipment, determined according to the needs of the space, can provide either heating or cooling in a 2-pipe system, while in a 4-pipe system, spaces can use both heating and cooling modes simultaneously. Schematic diagrams of the FCU System and VRF systems are shown in Figure 1 and Figure 2.

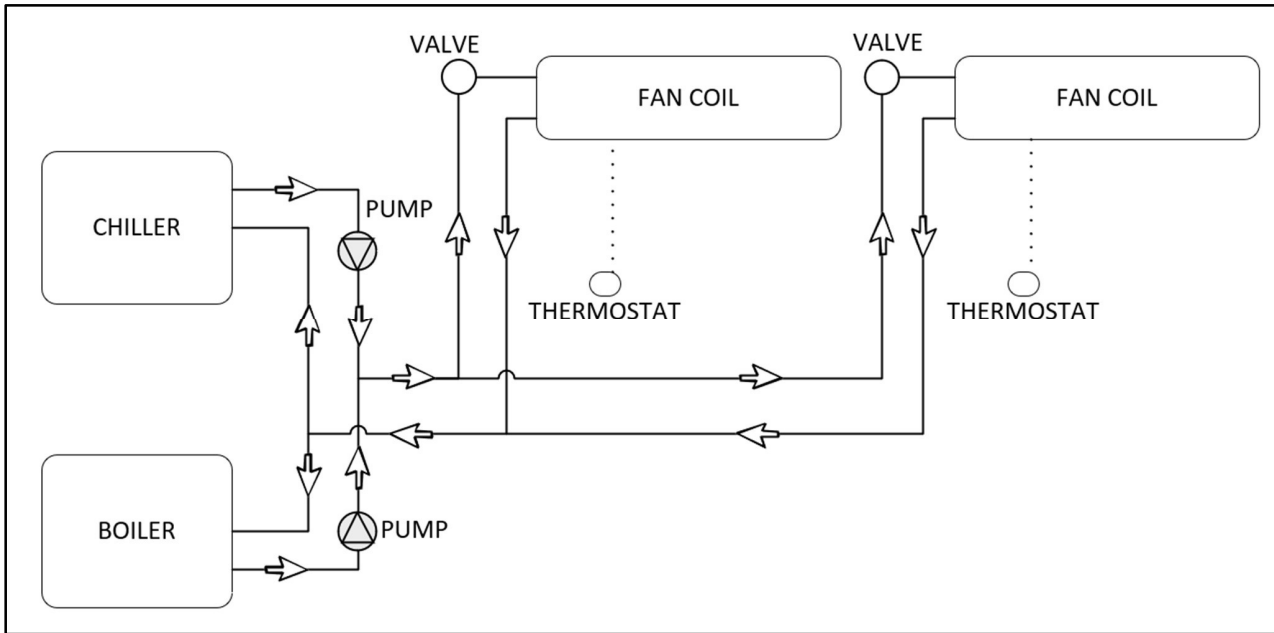


Figure 1.
FCU System Schematic Diagram

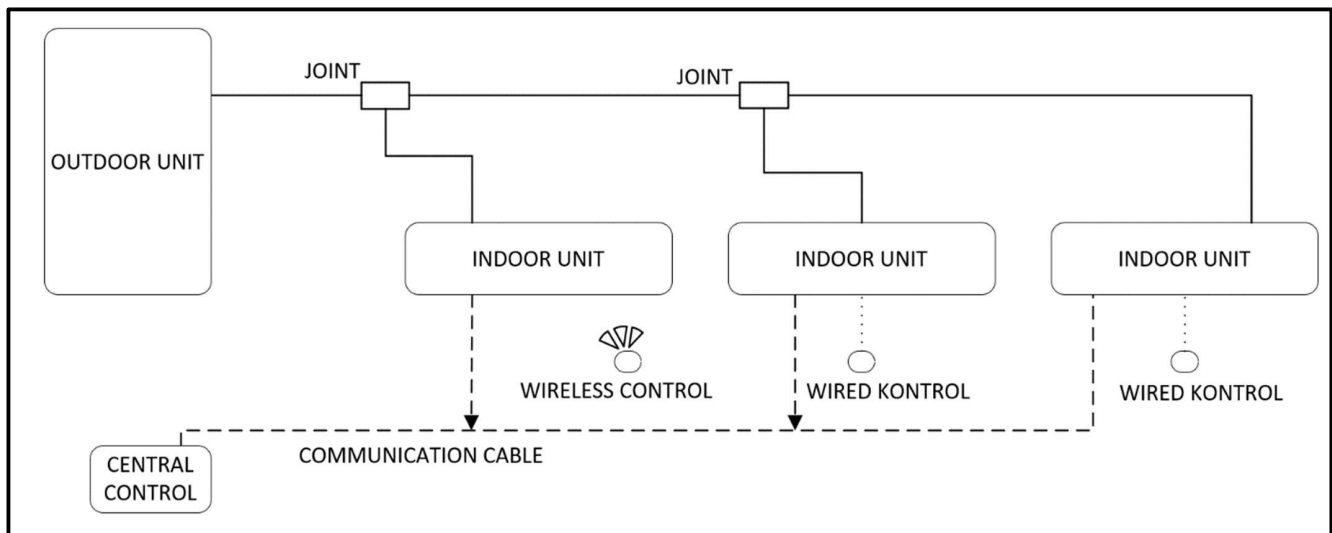


Figure 2.
VRF System Schematic Diagram

Extensive research has been conducted on VRF and FCU systems, and these studies continue. The findings obtained from examining these studies are summarized below.

Aynur et al. (2006) a study on VRF systems involving an office application, showed that the individual control mode provided more effective thermal control and higher thermal efficiency compared to the general control mode.

In their study on a VRF system with two indoor units, Park et al. (2001) studied how well a VRF system with electronic expansion valves worked and stressed how important it is to make the right adjustments to get the best performance out of the system.

Xia et al. (2002) in his study on a VRF system with five indoor units and a three-pipe structure, demonstrated that using two compressors in tandem increased the system's performance.

Masuda et al. (1991) by developing a new control methodology for a two-indoor-unit VRF system, stated that the independent control of indoor units increased energy efficiency.

Hai et al. (2006a) in his experimental studies on a 3-pipe VRF system with a 30 kW rated capacity, found that the system had high Coefficient of Performance (COP) values in simultaneous heating and cooling mode.

Hai et al. (2006b) in his research on a VRF system with a storage tank for ice, stated that integrating an ice storage tank increased energy efficiency by 25% and calculated a return on investment within 3 years considering electricity prices in Shanghai.

Özsoy et al. (2019) by examining the differentiation of air velocities and air distribution in fan coil systems, revealed that using an optimally designed distributor could contribute to achieving a more homogeneous air distribution.

Material and Methods

The General Features of the Building

The mentioned "1000-Person Male Student Dormitory" is located at Mersin University's Yenisehir campus in Mersin (Figure 3). The mechanical installation reports for the premises have been obtained from the Ministry of Youth and Sports of the Republic of Turkey.

In the current project, a traditional water heating and cooling system was preferred. To explain the traditional system, in the traditional system, boilers are used to heat the water and chillers are used to cool the water.

Boilers generally work with fuel (natural gas, fuel oil, biofuel, etc.) or electricity. The boiler produces heat by heating or evaporating water. This heat provides heating to the building or facility through a heating system. Boiler systems use energy from the combustion process to heat water and generally transfer heat by circulating the water in a loop.

Chillers are generally used in ventilation, air conditioning and cooling systems. Chillers cool an environment, usually using water or another refrigerant. Chillers work by circulating the refrigerant and allowing this fluid to exchange heat. Depending on the cooling load, chillers can use the condensation principle to cool the cooling water (with the help of a cooling tower) or use compressors to cool the cooling liquid.

AutoCAD project drawings, on the other hand, have been acquired from the project author. In the project, the selections for Fan Coil Units (FCU) have been made, and the selections for Variable Refrigerant Flow (VRF) devices are conducted in this study. The total enclosed area of the building is approximately 35000 square meters, comprising a total of 418 premises.

Operation calculations have been performed, taking into account both summer and winter conditions, as well as seasonal transitions.



Figure 3.
1000-Person Male Student Dormitory

VRF Indoor Unit Selection

The VRF device selections were made using a Daikin Xpress selection program. The device type selections were made as concealed ceiling type and cassette type of the same kind as the selected fan coils. Depending on the number of devices within the premises, one or more individual control selections were made. Since the FCU system in the project is two-pipe, for the sake of comparison and preference, the VRF system was also preferred as a two-pipe system. This means the system can operate in either heating or cooling mode simultaneously. Figure 4 and Figure 5 show the indoor unit types of VRF systems.



Figure 4.
Ducted Type VRF Indoor Unit

VRF Outdoor Unit Selection

During the selection of the outdoor units, the diversity ratio was taken into consideration in the system. However, due to the nature of the existing structure being a dormitory rather than a residential building, the diversity ratio was preferred to be minimal. The outdoor units have been selected according to the two-pipe system (Figure 6). The planned location for the outdoor units is in unused spaces at the top of the building.



Figure 5.
Cassette Type VRF Indoor Unit



Figure 6.
VRF Outdoor Unit

Determination of the Location of Copper Pipe Installation

In a VRF system, unlike the FCU system, there are specific rules for piping. The most crucial rule is that the copper pipe distance from the first indoor unit separation to the last indoor unit should not exceed 40 meters. Therefore, zoning has been implemented within each section of the building. Due to the limited number of indoor units that can be connected to each outdoor unit, zoning has also been implemented between floors.

Heat Loss and Gain Calculation, and Heating-Cooling Group Selections

The selections of the boiler chiller group, made based on the building's heat loss and gain charts and received from the project author, have been organized and presented in Table 1 and Table 2.

Table 1.
Boiler Capacity Selection

Boiler Capacity (Q_b)		
Heating zone 1	46300	kcal.h ⁻¹
Heating zone 2	51950	kcal.h ⁻¹
Heating zone 3	46150	kcal.h ⁻¹
Zone 1 FCU installation	98550	kcal.h ⁻¹
Zone 1 FCU installation	92300	kcal.h ⁻¹
Zone 1 FCU installation	112750	kcal.h ⁻¹
Kitchen fresh air AHU	35000	kcal.h ⁻¹
Boiler installation (Q)	1700000	kcal.h ⁻¹
Total heating requirement	2183000	kcal.h ⁻¹
Safety factor	5	%
Device capacity	2292150	kcal.h ⁻¹

3 quantity premix burner condensing boilers with 800000 kcal.h⁻¹ capacity were selected. 2 quantity air-cooled water chillers with a cooling capacity of 800 kw have been selected. (It will be able to meet the needs in the climatic conditions of the region.)

Table 2.
Chiller Capacity Selection

Chiller Capacity (Q_c)		
Zone 1 FCU installation	469650	kcal.h ⁻¹
Zone 2 FCU installation	540950	kcal.h ⁻¹
Zone 3 FCU installation	559150	kcal.h ⁻¹
Total cooling requirement	1569750	kcal.h ⁻¹
Coincident time factor	85	%
Device capacity	1334288	kcal.h ⁻¹

The list of devices specified in the project for the VRF system is shown in Table 3.

VRF System Zoning Plan

Zoning and outdoor unit (OU) selection capacities are provided in Table 4.

Ground floor plan zones are shown in Figure 7 and outdoor units are shown in Figure 8. Figure 9 shows an overview of the building.

Results

FCU and VRF System Operational Costs

After the selection of VRF system outdoor units, the one-year operational cost based on space requirements, seasonal COP and seasonal efficiency (SEER) values is shown in Table 5.

Based on the selections made for the boiler, chiller, and circulation pump in the project, the electricity consumption and

natural gas consumption for the gas-fired floor-standing boiler are calculated and the one-year operational cost is shown in Table 6-12.

The calculations do not take into account the electricity consumption of the indoor units in the systems, as they are significantly low compared to external factors. The calculations assume no consumption for 2 months, each representing the transition between the summer and winter seasons. The unit price of natural gas is considered 6.07 TLm⁻³, and the unit price of electricity is considered 4.62 TLkWh⁻¹. It is anticipated that instead of 3 units of 800000 kcal.h⁻¹ floor-standing natural gas boilers, 1 unit of 688000 kcal.h⁻¹ capacity floor-standing natural gas boiler will be used for hot water usage. The percentage-wise comparison of VRF operating costs is shown in Table 13.

Table 3.
Device Selection List

Description	Capacity(kW)	Quantity
4 way cassette	1.7	50
4 way cassette	2.2	8
4 way cassette	2.8	48
4 way cassette	3.6	25
4 way cassette	4.5	58
4 way cassette	5.6	18
4 way cassette	7.1	22
M.S.P hidden ceiling	2.8	14
M.S.P hidden ceiling	3.6	200
M.S.P hidden ceiling	4.5	95
M.S.P hidden ceiling	5.6	3
Outdoor unit	52	2
Outdoor unit	78.5	1
Outdoor unit	90	2
Outdoor unit	102.4	4
Outdoor unit	123.5	4
Outdoor unit	130	2
Outdoor unit	135	1
Outdoor unit	140.4	2
Outdoor unit	145.8	1
Outdoor unit	151.2	1
Joint		295
Joint		114
Joint		91
Joint		26
Expansion valve		2
Expansion valve		3
Expansion valve		5
Outdoor unit 2-joint		7
Outdoor unit 3-joint		11
Wired control		445
Central control		7

Table 4.
Zones and Capacities

Unit	HP	Location	Capacity(kW)	Unit	HP	Location	Capacity(kW)
OU-1	50	Ground floor left	63.8	OU-10	32	5th floor middle	46.6
		1st floor Left	79.7			6th Floor Middle	46.6
		Total	143.5			Total	93.2
OU-2	46	2nd floor left	69.4	OU-11	38	7th floor middle	46.6
		3rd floor left	64			8th floor middle	61.2
		Total	133.4			Total	107.8
OU-3	44	4th floor left	64	OU-12	32	1st basement floor right	91.4
		5th floor left	64				
		Total	128			Total	91.4
OU-4	44	6th floor left	64	OU-13	52	Ground floor right	69.6
		7th floor left	64			1st floor right	82.5
		Total	128			Total	152.1
OU-5	28	8th floor left	76.4	OU-14	48	2nd floor right	71.3
						3th floor right	65.9
		Total	76.4			Total	137.2
OU-6	54	2nd basement floor middle	19.7	OU-15	44	4th floor right	65.9
		1st basement floor middle	131.2			5th floor right	65.9
		Total	150.9			Total	131.8
OU-7	38	Ground floor middle	108.9	OU-16	46	6th floor right	65.9
		Total	108.9			7th floor right	65.9
OU-8	38	1st floor middle	109.7			Total	131.8
OU-9	50	2nd floor middle	52	OU-17	28	8th floor right	79.2
		3rd floor middle	46.6				
		4th floor middle	46.6				
		Total	145.2			Total	79.2

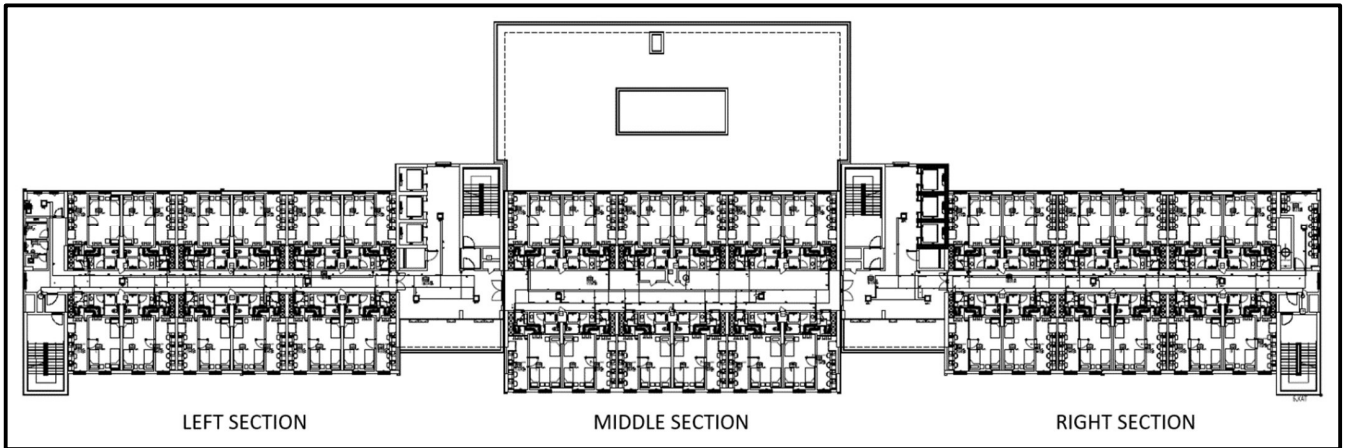


Figure 7.
Floor Plan Zones

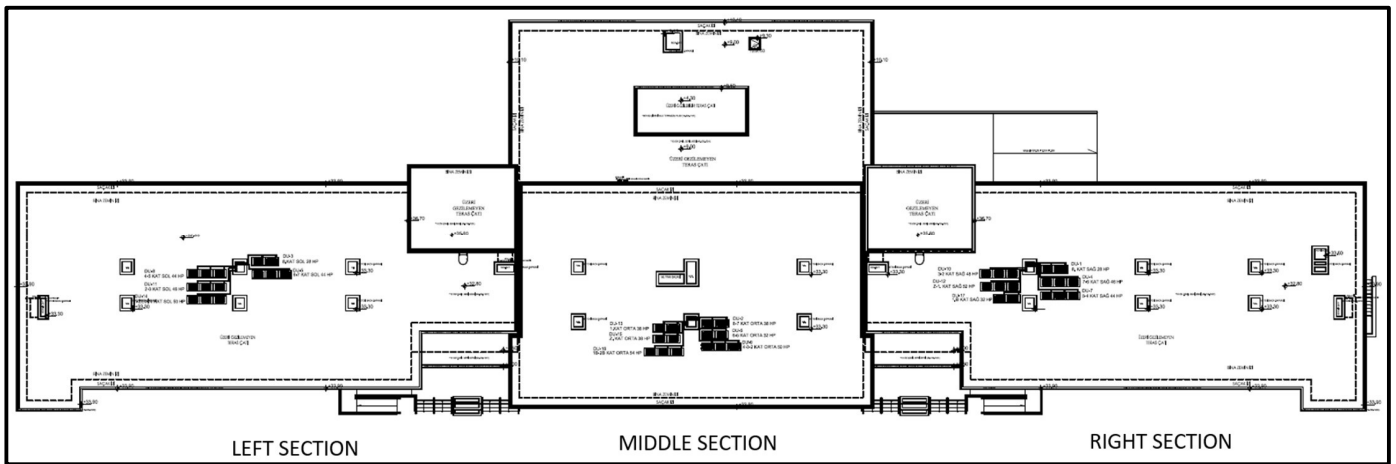


Figure 8.
Outdoor Unit Layout Plan



Figure 9.
Overview of and information about the building

Table 5.
Annual Operational Cost of the VRF System

Od unit name	SCOP	SEER	Cooling			Heating		
			Total capacity required (kW)	Total working (hour)	Total consumption (kWyear ⁻¹)	Total capacity required (kW)	Total working (hour)	Total consumption (kWyear ⁻¹)
DU-1	4.2	6.4	143.5	1200	26906.3	40.19	2100	20095
DU-2	4.1	6.4	133.4	1200	25012.5	40.18	2100	20580
DU-3	4.2	6.5	128.0	1200	23630.8	40.58	2100	20290
DU-4	4.2	6.5	128.0	1200	23630.8	41.49	2100	20745
DU-5	4.2	6.5	76.4	1200	14104.6	26.89	2100	13445
DU-6	4.3	6.4	150.9	1200	28293.8	22.20	2100	10841.9
DU-7	4.3	6.9	108.9	1200	18939.1	19.00	2100	9279.1
DU-8	4.3	6.9	109.7	1200	19078.3	21.80	2100	10646.5
DU-9	4.2	6.4	145.2	1200	27225	42.39	2100	21195
DU-10	4.2	6.4	93.2	8640	125820	28.65	2100	14325
DU-11	4	6.3	107.8	8640	147840	35.44	2100	18606
DU-12	4.3	6.4	91.4	1200	17137.5	25.57	2100	12487.7
DU-13	4.3	6.4	152.1	1200	28518.8	42.14	2100	20580
DU-14	4.1	6.4	137.2	1200	25725	41.09	2100	21046.1
DU-15	4.2	6.5	131.8	1200	24332.3	41.51	2100	20755
DU-16	4.1	6.4	131.8	1200	24712.5	41.71	2100	21363.7
DU-17	4.2	6.5	79.2	1200	14621.5	27.16	2100	13580
DX-1	4.0	5.9	57.0	1200	11593.2	10.0	2100	5250
DX-2	4.2	6.5	128.0	1200	23630.8	27.0	2100	13500
DX-3	4.0	5.9	0.0	1200	0.0	56.0	2100	29400
			Total electricity consumption (kWYear ⁻¹)			Total electricity consumption (kWYear ⁻¹)		
			650752.6			338010.9		
			Total working time			Total working time		
			1 year 5 month			1 year 5 month		
			1 month 30 day			1 month 30 day		
			1 day 8 hour			1 day 14 hour		
VRF installation heating & cooling annual energy cost (TL)	Total (kWyear⁻¹)		Electricity unit price (TLkW⁻¹)			Annual energy cost (TLyear⁻¹)		
	988763.5		4.62			4568087.39		

Table 6.*Circulation Pumps Total Consumption (Heating)*

	Flow (m^3h^{-1})	High pressing (mss)	Pump number (principal-reserve)	Pump power calculation (numberkW ⁻¹)	Pump power calculation (total kWh ⁻¹)
Boiler primary circuit	40	5	3P	1.00	3.00
Towel warmer	8	10	1P +1R	0.30	0.30
Fan coil	20	10	1P +1R	1.00	1.00
Ahu heating installation	2	10	1P +1R	0.30	0.30
Total consumption (kW)					4.60

Table 7.*Natural Gas Consumption (Heating)*

Boiler capacity (kW)	1990	Working days per month	30
Natural gas lower heating value (kcal.h ⁻¹)	8.250	Working months per year	5
Boiler efficiency (%)	85	Annual consumption (m ³ year ⁻¹)	512504.81
Consumption (m ³ h ⁻¹)	244.05	Natural gas unit price (TLm ⁻³)	6.07
Daily working hour	14	Annual energy cost (TLyear ⁻¹)	3110904.21

Table 8.*Circulation Pumps Annual Energy Cost (Heating)*

	Hourly pump consumption (kWh ⁻¹)	Daily working hours	Days worked per month	Month worked per year	Annual consumption (kWyear ⁻¹)	Electricity unit price (TLkW ⁻¹)	Annual energy cost (TLyear ⁻¹)
Circulation pumps total consumption	4.60	14	30	5	9660	4.62	44629.20

Table 9.*Circulation Pumps Total Consumption (Cooling)*

	Flow (m^3h^{-1})	High pressing (mss)	Pump number (principal- reserve)	Pump power calculation (numberkW ⁻¹)	Pump power calculation (total kWh ⁻¹)
FCU	80	20	4P+1R	6.50	26
Chiller group	70	16	4P+2R	5.00	20
Total Consumption (kW)					46

Table 10.*Circulation Pumps Annual Energy Cost (Cooling)*

	Hourly pump consumption (kWh ⁻¹)	Daily working hours	Days worked per month	Month worked per year	Annual consumption (kWyear ⁻¹)	Electricity unit price (TLkW ⁻¹)	Annual energy cost (TLyear ⁻¹)
Circulation pumps total consumption	46	8	30	5	55200	4.62	255024

Table 11.*Chiller Annual Energy Cost*

Chiller capacity (kW)	1600	Month worked per year	5
Energy Efficient Ratio (EER)	3.0	Annual consumption (kWyear ⁻¹)	640000
Consumption (kW)	533.33	Electricity unit price (TLkW ⁻¹)	4.62
Daily working hours	8	Annual energy cost (TLyear ⁻¹)	2956800
Days worked per month	30		

Table 12.*FCU System Annual Energy Cost*

Consumption name	Annual energy cost (TLyear ⁻¹)
Natural gas consumption (heating)	3110904.21
Circulation pumps annual energy cost (heating)	44629.20
Circulation pumps annual energy cost (cooling)	255024
Chiller annual energy cost	2956800
Total energy cost	6367357.41

Table 13.*Annual Operating Cost Analysis for VRF and FCU Systems*

VRF installation heating & cooling annual energy cost (TL)	FCU system annual energy Cost (TL)	Annual energy cost difference (TL)	With VRF system annual energy savings (%)
4568087.39	6367357.41	1799270.03	28%

Conclusions

VRF systems have a more professional structure with mass production and an extensive service network. The assembly processes are carried out by authorized services designated by the manufacturing companies, using copper pipes produced in factories. On the other hand, FCU system equipment and piping processes are also performed by authorized personnel. Labor in FCU systems requires more human skills compared to VRF systems, leading to a higher likelihood of manufacturing errors. This indicates that both systems have different assembly and production processes.

VRF systems tend to offer more advantageous prices in terms of initial investment costs since they have single-firm production. On the other hand, the components that make up the FCU system may face more time and cost challenges in material procurement during the operation process since they cannot be supplied by a single company. The higher number of components in the FCU system also requires more technical personnel. In FCU systems, the fresh air needs in the spaces can be met using a DX coil heat recovery device instead of a water coil heat recovery device. DX coil outdoor units are also selected for air handling units in this study.

When considering the annual operating expenses for both systems, the calculated annual operating cost for the VRF system

is 4568087.39 TL, while for the FCU system, it is 6367357.41 TL. The calculated operational cost difference between the two systems is 1799270.03 TL annually.

Considering all these factors, it can be said that VRF systems are more efficient in terms of energy consumption and operational ease compared to central heating and cooling systems.

Peer-review: Externally peer-reviewed

Author contributions:

Ö.F.K.: Data curation, original draft preparation, investigation, analysis

N.A.: Supervision, literature search, writing manuscript, methodology.

Financial disclosure: This research received no external funding.

Conflict of Interest: The author has no conflicts of interest to declare.

References

- Aynur, T.N., Hwang, Y., & Radermacher, R. (2006). *Field Performance Measurements of a VRV AC/HP System*, 11th International Refrigeration and Air Conditioning Conference, Purdue, IN-USA, 1-8.
- Hai, X.H., Jun, S., Hand, Z.Y., & Bin, T.C. (2006a). *Design and research of the digital VRV multiconnected units with three pipes type heat recovery system*, 11th International Refrigeration and Air Conditioning Conference, IN, USA, 1-5.
- Hai, X.H., Tao, Z., Yun, F.H., & Jun, S. (2006b). *Design and research of the commercial digital VRV multi-connected units with sub-cooled ice storage system*, 11th International Refrigeration and Air Conditioning Conference, IN, USA, 1-5.
- Masuda, M., Wakahara, K., & Matsuki, K. (1991). Development of a multi-system air conditioner for residential use. *ASHRAE Transactions*, 97(2), 127-131.
- Özsoy M., Yücel C., Varlıca O., Kılıç S., & Kaplan, K. (2019). Optimization of Air Distribution in A Non-Ducted Concealed Type Fan Coil Unit Heat Exchanger, 5 (3), 124-130.
- Park, Y.C., Kim, Y.C., & Min, M.K. (2001). Performance analysis of a multi-type inverter air conditioner, *Energy Conversion and Management*, 42 (13), 1607–1621.
- Xia, J., Winandy, E., Georges, B., & Lebrun, J. (2002). *Testing methodology for VRF systems*, 9th International Refrigeration and Air Conditioning Conference, Purdue, IN, USA, 1-8.



Numerical Investigation of The Flow Structure on Ground Surface Mounted Square Prism

Zemin Yüzeyine Monte Edilmiş Kare Prizma Üzerindeki Akış Yapısının Sayısal Olarak İncelenmesi

Onur KÜÇÜKKURT



Atatürk University, Faculty of Engineering, Mechanical Engineering Erzurum, Türkiye .

Cuma KARAKUŞ



Iskenderun Technical University, Faculty of Engineering and Natural Sciences, Mechanical Engineering. Iskenderun, Türkiye.

ABSTRACT

The three-dimensional flow structure on a square prism mounted on a horizontal ground was investigated numerically using the Ansys Fluent program for Reynolds number $Re = 250, 2500$ and $2.5 * 10^6$, using the Standard $k-\epsilon$ turbulence model equations. In the study, a square prism with a large Depth Ratio ($DR = 4$) was used. As a result, the information was obtained about the characteristic structure of the flow around the object. For $z/h = 0.05, 0.5, 0.75$ and 1 , the top views of the Streamlines and Turbulent kinetic energy data formed behind the ground surface-mounted square prism are shared. Streamlines and Turbulent kinetic energy side views formed in the front, top and rear flow regions of the ground surface-mounted square prism for $y/D = 0, 0.25, 0.5, 0.75, 1$ and 1.25 are presented. On the prism surfaces, the structure of the upstream and downstream flow changed due to separation from the prism front surface and reattachment of the flow. This situation revealed the effect of the Depth Ratio on the structure of the flow topology on the object by changing the drifting flow structure and turbulent kinetic energy structure in the wake region. As the Reynolds number acting on the prism increased, the size of the vortex decreased noticeably.

Keywords: 3D Square Prism, Separated Flows, Turbulence Simulation

ÖZ

Yatay bir zemin üzerine monte edilmiş kare prizma üzerindeki üç boyutlu akış yapısı Standard $k-\epsilon$ türbülans modeli denklemlerinden yararlanılarak Reynolds sayısı $Re = 250, 2500$ ve $2.5 * 10^6$ için Ansys Fluent programı kullanılarak sayısal olarak araştırılmıştır. Çalışma da büyük derinlik oranı, ($DO=4$) kare prizma kullanılmıştır. Sonuç olarak cisim etrafında oluşan akışın karakteristik yapısı hakkında bilgi sahibi olunmuştur. $z/h = 0, 0.5, 0.75$ ve 1 için zemin yüzeye monte kare prizma arkasında oluşan Akım çizgileri, Türbülans kinetik enerji verileri üst görünüşleri paylaşılmıştır. $y/D = 0, 0.25, 0.5, 0.75, 1$ ve 1.25 için zemin yüzeye monte kare prizma ön, üst ve arka akım bölgesinde oluşan Akım çizgileri, Türbülans kinetik enerji yan görünüşleri sunulmuştur.

Prizma yüzeyleri üzerinde, prizma ön yüzeyinden ayrılmış ve akışın yeniden bağlanması nedeniyle yukarı ve aşağı yönlü akışın yapısı değişmiştir. Bu durum iz bölgesindeki sürüklenen akış yapısını ve türbülans kinetik enerji yapısını değiştirmek vasıtasıyla derinlik oranının cisim üzerindeki akış topolojisinin yapısına etkisini ortaya koymuştur. Prizma derinlik oranının artmasıyla girdabın büyüklüğü gözle görünür oranda azalmıştır.

Anahtar kelimeler: 3 Boyutlu Kare Prizma, Akış Ayrılması, Türbülans Simülasyonu



Received/Geliş Tarihi : 13.05.2024
Accepted/Kabul Tarihi : 06.06.2024
Publication Date/Yayın Tarihi : 30.06.2024

Corresponding Author/Sorumlu Yazar:
Cuma KARAKUŞ
E-mail: cuma.karakus@iste.edu.tr

Cite this article: Küçükkurt, O., Karakuş C., (2024). Numerical Investigation of The Flow Structure On Ground Surface Mounted Square Prism, *Journal of Energy Trends*, 1(1), 21–32.



Content of this journal is licensed under a Creative Commons Attribution-Noncommercial 4.0 International License.

Introduction

In engineering sciences, the complex structure of flow over objects has been a subject of great curiosity in every field from the past to the present. It has been investigated in various fields of engineering, and its results have been considered in the literature. The desire to know the relationship between the fluid in motion and the object it comes into contact with has always kept the interest of researchers in this subject up to date. Numerical studies carried out using developed various software make it possible to study the pressure fields, vortex structures and vortex-induced effects of objects with complex geometries as a result of their interaction with the fluid in a shorter time and with less cost compared to experimental studies. Since real-scale investigations are very time-consuming, laborious, and costly, numerical studies provide the opportunity to reach the results in a shorter time compared to experimental studies.

If the streamlines of the flow around a body remain constant along the surface of the body and flow fields and flow separations occur on the back surface of the body, the body is aerodynamically considered to be a blunt body. Blunt bodies called 'pressure drag' are subjected to the effect of pressure drag, which is part of the total drag. Liu (2019) Blunt bodies, which are frequently used in industrial and engineering applications, are cylinders, square prisms, rectangular prisms, or spheres. The blunt body shown in Figure 1 provides information about the structure of the flow for different conditions, such as vortex intensity, vortex types, separation zone, reattachment zone, horseshoe vortex structures. In addition to the Reynolds number (Re), the shape, size, and the Depth Ratio, L/D (length/width), (DR) of the body are of great importance in the generation of these flow topologies.

In many engineering applications, the problem of flow over blunt objects such as square cylinders, circular cylinders, etc. is quite common. Flow separation, vortex shedding frequency, drag, etc. problems affecting flow are of great importance in revealing flow and aerodynamic properties due to their direct effects on engineering applications (Durhasan, 2020).

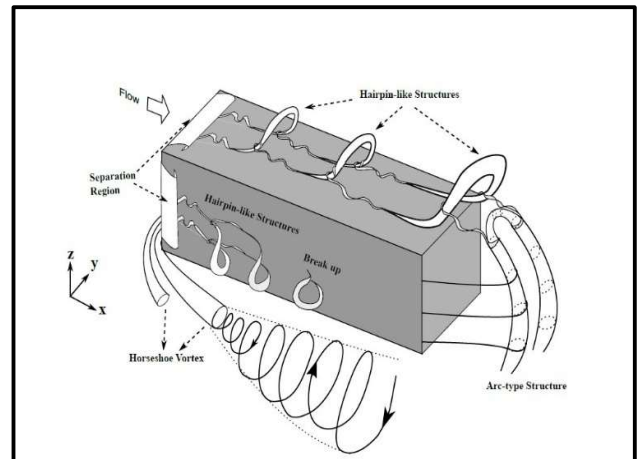


Figure 1.
Vortex structures of a long square cylinder (Zargar, 2020).

(Gao & Chow, 2005) investigated numerically two-dimensional flow over a cube. They used the Navier-Stokes Reynolds Averaged turbulence model (RANS) as the turbulence model. The aim of the study was to determine the levels of flow separation, separation and reattachment in the corner at the top of the cube. As a result, they emphasized that obtained Turbulent Kinetic Energy (TKE) values, flow separation and reattachment distances are consistent with experimental studies. Tauqeer et al. (2017) examined numerically the flow over two-dimensional square, triangular, semicircular objects using (RANS) equations. In their study, the Reynolds number was taken as $Re = 10^6$, while the boundary layer thickness was taken between 0.73-2.55. As a result, it is emphasized that the numerical model results are compatible with the published literature studies with high Reynolds number conducted experimentally. Korukcu (2020) analyzed the flow over a single square cylinder in two dimensions. He investigated the effect of blockage ratio ($\beta=B/H$) on the laminar continuous flow regime with the $Re=40$ and heat transfer. He used ANSYS CFX 14.0 in his calculations. The drag coefficient (C_d), friction coefficient (C_f), Nusselt number (Nu) on the square cylinder surfaces increased as the blockage ratio increased. Zargar et al. (2021) numerically studied the flow around a wall-mounted square prism and a square prism with a long DR for the $Re=50-250$. They emphasized that the vortex size decreases drastically when the DR changes. When the coefficients of friction and buoyancy are analyzed, it is found that the DR square prism is more affected than the square prism. (Wang & Lam, 2021) investigated the flow structure around a wall-mounted short square cylinder with aspect ratio ($AR, H/D$)=2 using experimentally Particle Image Velocimetry (PIV) and numerically Large Eddy Simulation (LES) turbulence model. In their study, they compared the experimental and numerical results of the time-averaged velocity vectors, the TKE values. As a result, they revealed that there is a difference between the PIV and the LES results in TKE

values. They stated that the Karman vortex structure is experimentally and numerically compatible. Zerrin (2021) examined numerically the structure of the flow around a square cylinder in a vertical channel for three different Reynolds numbers ($Re = 100, 150, 200$). Ansys Fluent software was utilized for the solution of the numerical study. She revealed that integrated heat transfer affects the flow along the channel under laminar regime conditions. (Kucukkurt & Karakus, 2024) in their study, the flow structure on the cube with $AR=1$ was analyzed three dimensionally and numerically. They presented information about the flow structure for Reynolds number $Re=250$. As a result, it is understood that has a complex structure consisting of the combination of many vortex systems depending on the Reynolds number and the shape of the cube.

Understanding the vortex dynamics of the flow around massive objects is very valuable in device design and in knowing the wind loads on architectural structures. As a result of the examination of the flow structure on the objects, it provides convenience in solving possible problems that arise or may arise in engineering applications such as high-rise buildings, bridge piers, blast furnace chimneys, truck trailers, container yards, and microchips (Goswami & Hemmati, 2023).

Flow structures formed on containers due to non-permanent wind loads in port areas may cause containers to overturn and get damaged from time to time. At the same time, it causes environmental pollution and accumulation due to the flow structure in the port areas. Therefore, it is of great importance to numerically investigate the flow structure on single- or multi-row containers and to know the flow structure. When the literature is examined, no numerical study has been found for a value of $2.5 \cdot 10^6$ of the Reynolds number representing the flow on containers in port areas.

In this study, in order to simulate the flow structure on containers resembling the basic geometric shape of a square cylinder in port areas, the flow on the model with the $DR = 4$, which gives the ratio of container length (L) to width (D), is numerically examined. Firstly, the study was carried out for the value of Reynolds number, $Re=250$ depending on the square cylinder width representing very low speeds, $Re=2500$ representing medium speeds, and finally for the value of Reynolds number $2.5 \cdot 10^6$ by taking the flow velocity as 25m/s , which is the maximum wind speed in the port area. In this study, the flow structure on a 2m width, 2m height and 8m length ground surface mounted square prism with $DR=4$ is numerically calculated using Ansys Fluent program for three different $Re = 250, 2500$ and $2.5 \cdot 10^6$. The flow structure in front of, on and behind the ground surface mounted square prism is analyzed.

Material and Methods

The numerical analysis flow field dimension values of the problem are shown in Figure 2. Flow analysis was performed for a square prism placed in a channel with dimensions of $11D \times 5D \times 34D$. The width of the ground surface-mounted square prism is taken as $D = 2\text{m}$. Information about the views of the flow on the ground surface mounted square prism in x-y-z coordinate planes is presented also in Figure 2. The ground surface mounted square prism on the channel is assumed to be exposed to the fluid at velocity U . The velocity value was calculated for Reynolds number $Re = 250, 2500$ and $2.5 \cdot 10^6$. When the literature studies are examined, it is evident that fluid air or water is used in the studies. In this study, air was used as a fluid. The ambient temperature was taken as 20 degrees Celsius. In the study, the mesh number was considered to be $2\,753\,431$ for all Reynolds numbers. Skewness and orthogonal mesh quality value was obtained as $0.22, 0.90$ respectively. Peyvandi (2024) In his study, he used the skewness value between $0.20-0.22$ when defining the quality of the network structure. This value range is considered to be very good in Ansys user manual. A standard k- ϵ turbulence model was used to determine the flow structure.

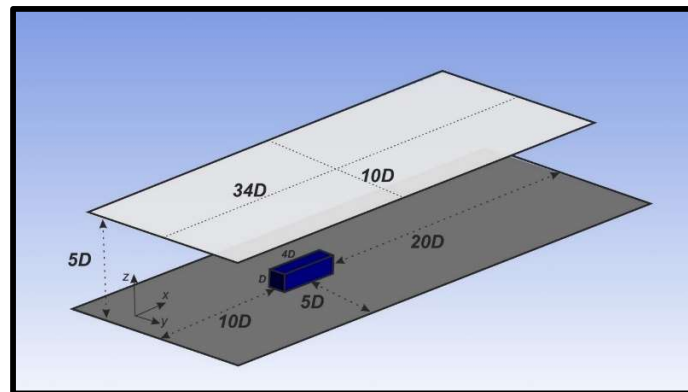


Figure 2.
Numerical analysis flow field dimensions

Standard k- ϵ Turbulence Model

The standard k- ϵ turbulence model is a common method used in practical engineering flow applications to determine both the turbulence length and time scale by solving two separate equations. It has become the preferred solution method for turbulent flow simulations by researchers because it provides economical, stable, and highly accurate results. The standard k- ϵ turbulence model is an approximation model that uses mathematical calculations for the turbulent kinetic energy and its dissipation rate (Rusdin, 2017).

Transport Equations for the Standard k-ε Model

This model proposed by Kolmogorov presents the equations of turbulence kinetic energy transport and its dissipation rate in

$$\frac{\partial}{\partial t}(\rho k) + \frac{\partial}{\partial x_i}(p k u_i) = \frac{\partial}{\partial x_j} \left[\left(\mu + \frac{\mu_t}{\sigma_k} \right) \frac{\partial k}{\partial x_j} \right] + G_k + G_b - \rho \varepsilon - Y_M + S_k \quad (1)$$

$$\frac{\partial}{\partial t}(\rho \varepsilon) + \frac{\partial}{\partial x_i}(p \varepsilon u_i) = \frac{\partial}{\partial x_j} \left[\left(\mu + \frac{\mu_t}{\sigma_\varepsilon} \right) \frac{\partial \varepsilon}{\partial x_j} \right] + C_{1\varepsilon} \frac{\varepsilon}{k} (G_k + C_{3\varepsilon} G_b) - C_{2\varepsilon} \rho \frac{\varepsilon^2}{k} + S_\varepsilon \quad (2)$$

Here; k is the turbulence kinetic energy, ε is the dissipation velocity, and G is the turbulence kinetic energy production due to the velocity gradients of buoyancy. σ_k and σ_ε denote the turbulence Prandtl number for k and ε , respectively. Y_M denotes the contribution of fluctuating dilatation to the overall dissipation rate in compressible turbulence. S_k and S_ε are user-defined source terms. $C_{1\varepsilon}$, $C_{2\varepsilon}$, C_μ in the equations are the turbulence Prandtl number constants. σ_k and σ_ε are the turbulence Prandtl number for k and ε , respectively. Shaheed et al. (2019)

Modeling Turbulent Viscosity

The viscosity of turbulent (eddy) flow is found by calculating μ_t (Modesti, 2020).

$$\mu_t = \rho C_\mu \frac{k^2}{\varepsilon} \quad (3)$$

Model Constants

$C_{1\varepsilon}$, $C_{2\varepsilon}$, C_μ are the turbulent flow Prandtl number constants.

$$C_{1\varepsilon}=1.44, \quad C_{2\varepsilon}=1.92, \quad C_\mu=0.09, \quad \sigma_k=1, \quad \sigma_\varepsilon=1.3$$

These default values were determined from experiments for basic turbulent flows often encountered in shear flows, such as layered flow structures and jets. They have been found to work quite well for a wide range of wall-bound and free shear flows (Ansys Fluent Theory Guide).

Equation (1) and Equation (2). The value of the turbulence kinetic energy is determined by calculating the mean velocity gradients Chen et al. (2024)

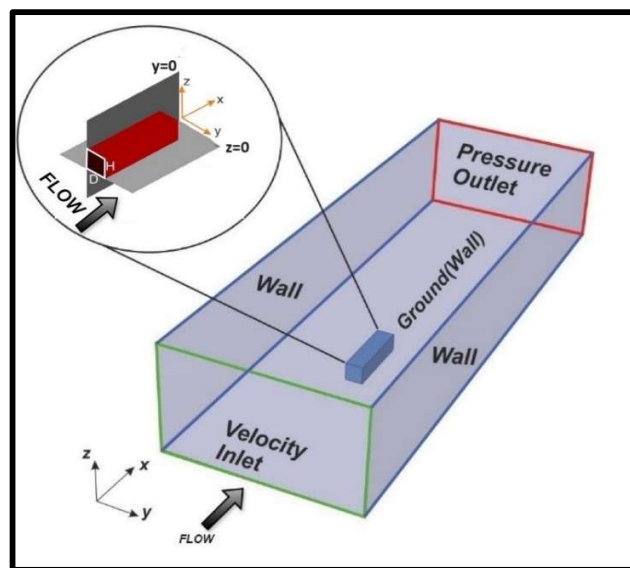


Figure 3.

Boundary conditions of the geometry in this study

The layout of the three-dimensional flow field for the ground surface-mounted square prism is shown in Figure 2 and Figure 3. The boundary conditions valid in the three-dimensional flow field on the ground surface mounted square prism are shown in Figure 3. In the selection of boundary conditions, preferences were made in accordance with the literature. Velocity inlet at the inlet and pressure outlet at the outlet ground surface and walls on the sidewalls were selected. A non-slip condition was applied to the side walls. As seen in Figure 3, the plane starting from the left side of the object is the $y = 0$ plane, the plane starting from the base is the $z = 0$ plane, and the distances $y / D = 0$ and $z / H = 0$ are the positions in the image.

Inlet:

$$u = U_{\infty}, T = T_{\infty} \tag{4}$$

Top and bottom walls:

$$u = U_{\infty}, v = 0, T = T_w \tag{5}$$

Square prism walls:

$$u = 0, v = 0, T = T_w \tag{6}$$

Outlet:

$$\frac{\partial u}{\partial x} = 0, \frac{\partial v}{\partial y} = 0, \frac{\partial T}{\partial x} = 0 \tag{7}$$

T_w is the temperature of the square prism wall, and T_{∞} is the temperature of the incoming fluid at the boundary conditions. Reynolds number $Re = \frac{U_{\infty} \cdot D}{\nu}$. Where U_{∞} is the free flow velocity of the fluid in the channel, D is the width of the square prism mounted on the ground surface, and ν is the kinematic viscosity.

In order to obtain mesh-independent solutions, experiments were carried out with different numbers of mesh structures. With the network layout created in this way, the network-independent solutions in the calculation area were defined as fine, medium, and coarse network layouts, and it was observed that the results were more consistent for the coarse network structure. (Yüce & Pulat, 2017) similarly emphasized that the method created with coarse mesh is consistent.

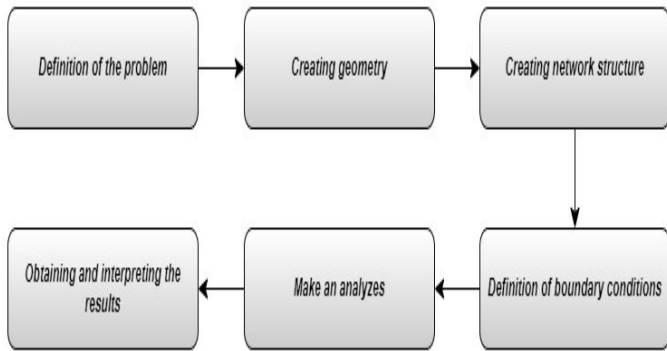


Figure 4.
Numerical analysis flow diagram

Numerical analysis flow diagram is shown Figure 4 that the flowchart of the method applied throughout the numerical study. For the numerical solutions of the three-dimensional flow field around the ground surface mounted square, the three-dimensional model was created in SolidWorks 12.0 drawing program and then imported into ANSYS. A mesh was applied to the model and boundary conditions were defined as shown in Figure 3. The Standard k-ε turbulence model was used in the numerical solution. The standard Wall Function was preferred as the wall approximation. The analysis of the model was run in

FLUENT 22.1 Academic program within Erzurum Atatürk University. The results obtained are discussed in the research and discussion section.

Results

In this study, the Reynolds numbers $Re = 250, 2500$ and $2.5 * 10^6$ for the flow through a $2m \times 2m \times 8m$ square prism with the $DR = 4$ mounted on a plane are numerically investigated. In the numerical study, the flow structure is investigated for three different cases: upstream of the ground surface mounted square prism, at the free surface of the square prism and downstream of the ground surface mounted square prism. In addition, side views of the streamlines and distribution TKE images of the flow through the front, top and back surfaces of the object at $y/D = 0, 0.25, 0.5, 0.75, 1$ and 1.25 and top views of the streamlines and TKE images of the flow through the object at $z/h = 0.05, 0.5, 0.75$ and 1 are presented. The flow direction is from left to right in all images. The streamlines of the resulting vortex show negative vortices rotating clockwise and positive vortices rotating counterclockwise.

The side views of the front top and back of the ground surface mounted square prism at $y/D=0, 0.25, 0.5, 0.75, 1$ and 1.25 are given in Figure 5. The left column shows that the time-averaged streamlines at the front of the ground surface mounted square prism, the middle column shows that the time-averaged streamlines at the top of the ground surface mounted square prism and the right column shows that the time-averaged streamlines at the back of the ground surface mounted square prism. The horseshoe vortex is formed in front of the object at equal distance. The horseshoe vortex distances are equal for $y/D=0, 0.25, 0.5, 0.75, 1$ and 1.25 , and the horseshoe vortex structure is $0.55D$ for $Re = 250, 0.29D$ for $Re = 2500$, and $0.21D$ for $Re = 2.5 * 10^6$. The results show that as the Reynolds number increases, the horseshoe vortex distance in the front region of the square prism decreases. When the images are analyzed, it is seen that the horseshoe vortex structure formed at the front of the square prism mounted on the ground surface at a distance of $y/D= 0.5$ for three $= 250, 2500$ and $2.5 * 10^6$ is more stable. Due to the onset of flow separation and the increasing pressure action on the surface of the free end of the square prism, the vertical plane midpoint moves downstream towards the surface of the square prism to form a separation bubble and reverse flow region. At the same time, shear layers can be seen between the separation bubble and the free flow region formed on the free surface of the ground surface mounted square prism. It is clearly seen that the “separation bubble” and the reverse flow region are formed due to the pressure increase along the upper surface of the prism on the offensive edge of the free end of the ground surface mounted square prism. As stated in Polat et al.

(2022) the presence of a separation bubble on the free surface of the ground surface-mounted square prism is observed due to the effect of the acceleration zone starting from the upper left edge of the body and extending along the x-axis. For $Re = 250$, the presence of a separation bubble and reverse flow region at $y/D = 0.75$ distance is clearly seen, while no stable structure is formed for other distances. For the $Re = 2500$ in the middle column, the presence of separation bubble and reverse flow regions for the distances $y/D = 0.25, 0.5$ and 0.75 is clearly seen. Depending on the height of the Reynolds number, it is seen that the vortex structure is more splayed and severe for the separation bubble formed on the free surface of the ground surface mounted square prism at $Re=2500$ compared to the separation bubble formed at $Re=250$. For $Re = 250, 2500$ and 2.5×10^6 , the separation bubble sizes formed on the ground surface mounted square prism were measured as $1.04D, 2.01D$ and $2.26D$, respectively. Behind the free surface mounted square prism, a reverse flow region and a saddle point at some distances are observed. At $Re=250$, the saddle point was measured as $1.17D$ for $y/D=0.25$, $2.05D$ for $y/D=0.5$ and $1.42D$ for $y/D=0.75$. Saddle points could not be measured for distances $y/D=0, 1$ and 1.25 . At $Re=2500$, this distance was measured as $0.9D$ for $y/D=0.25$, $1.6D$ for $y/D=0.5$, $1.35D$ for $y/D=0.75$ and $0.4D$ for $y/D=1$. Saddle points could not be measured for $y/D=0$, and 1.25 distances. At $Re=2.5 \times 10^6$, the saddle points were measured as $1.06D$ for $y/D=0.25$, $1.53D$ for $y/D=0.5$ and $0.83D$ for $y/D=0.75$. Saddle points could not be measured for $y/D=0, 1$ and 1.25 distances. When the saddle point distances in the back region of the square prism are analyzed, it is seen that the saddle point distance decreases for almost all distances as the Reynolds number increases. Kawahii et al. (2012) stated that as the aspect ratio of the body increases, the vortex length behind the body decreases and the saddle point approaches the body. In the present study, the increase in the Reynolds number shows that the saddle point distance decreases as the aspect ratio increases. Figure 6 shows the TKE values for the ground surface mounted square prism at $y/D=0, 0.25, 0.5, 0.75, 1$ and 1.25 and the time-averaged velocity vectors at these distances with side views. TKE values are presented for $Re=250$ in the left column, $Re=2500$ in the middle column and $Re=2.5 \times 10^6$ in the right column. When the TKE graphs are examined, it is determined that the value of the negatively rotating equilevel curves formed at the free surface trailing edge increases and is directed downwards behind the ground surface mounted square prism. However, the presence and intensity of the positively rotating vortex along the back surface of the ground surface-mounted square prism and along the downstream direction of the ground surface-mounted square prism and the plane plate junction region are observed to increase. It is observed that the maximum TKE value for $Re=250, Re=2500$ and 2.5×10^6 , occurs in the free surface escape region of the square prism at $y/D=0.5$

distance. The vortex distribution is clearly observed for all distances. When Figure 6 is examined, as stated in Özmen et al. (2014) the TKE value in the rear region of the ground surface mounted square prism continues to decrease from the junction point. When the time-averaged velocity vectors are analyzed, it is observed that the areas with high intensity velocity vectors on the free surface trailing edge side of the ground surface mounted square prism show areas where the velocities increase, while the areas with low intensity velocity vectors show areas where the velocities decrease or stop.

The top views of the flow through the ground surface mounted square prism for $z/h = 0.05, 0.5, 0.75$ and 1 distances are given in Figure 7. When the streamlines formed at $z/h = 0.5$ distance are examined, it is seen that the expected symmetrical structure is not formed for $Re = 2500$. For $Re=250$ and $Re= 2.5 \times 10^6$, it is seen that the vortex structure formed in the rear region of the ground surface mounted square prism is symmetrical and stable. For $z/h=0.5$ distance, the presence of one saddle point is observed at all Reynolds numbers. The saddle point at $z/h=0.5$ distance is $1.55D$ for $Re=250$, $0.76D$ for $Re=2500$ and $1.23D$ for $Re= 2.5 \times 10^6$. When the ground surface mounted square prism side surfaces are examined, it is seen that the vortex structure formed at $z/h= 0.5$ for $Re= 2.5 \times 10^6$ is symmetric and stable. It is understood that the vortex structure formed at $z/h=0.75$ for the same Reynolds number is not symmetric but still stable. For $Re=250$ and $Re=2500$, it is seen that the vortex structures formed on the side surfaces of the square prism mounted on the ground surface are not symmetrical and do not show stability.

The TKE top view passing through the square prism for $z/h=0.05, 0.5, 0.75$ and 1 is shown Figure 8. The TKE values of the flow through the ground surface mounted square are presented for distances $z/h = 0.05, 0.5, 0.75$ and 1 . When the maximum TKE values are examined, it is seen that it occurs at $z/h=0.5$ distance for $Re=250$. The maximum TKE value occurred at $z/h=0.75$ for $Re=2500$ and at $z/h=0.5$ for $Re= 2.5 \times 10^6$. The TKE values show that for all Reynolds numbers at $z/h=0.5$ and 0.75 distance, the vortex structures on the square prism side surfaces are more stable, become sharper and the sweeping process along the square prism side plane dominates.

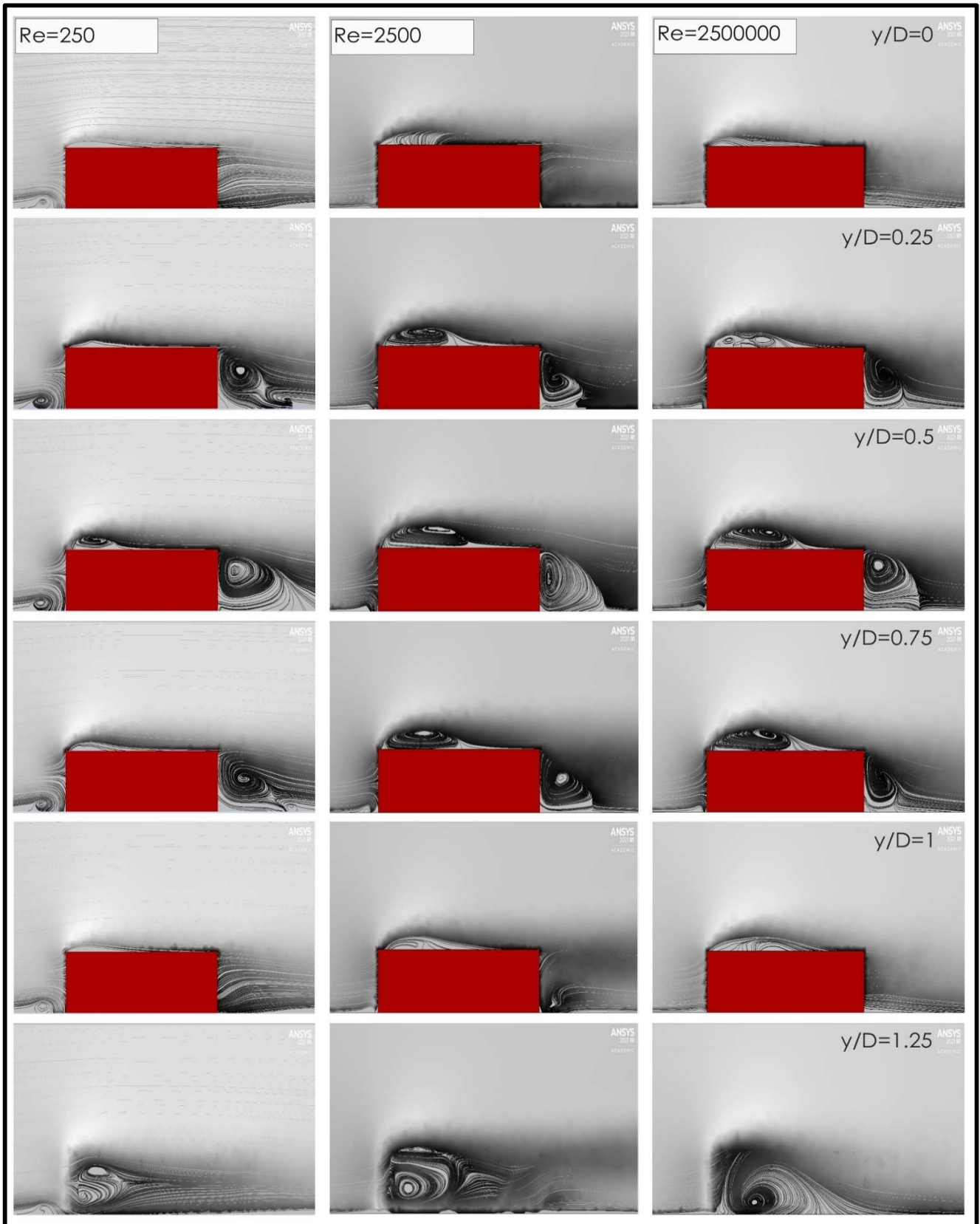


Figure 5.

Side view of the streamline formed at the front, top and back of the square prism for $y/D=0, 0.25, 0.5, 0.75, 1$ and 1.25

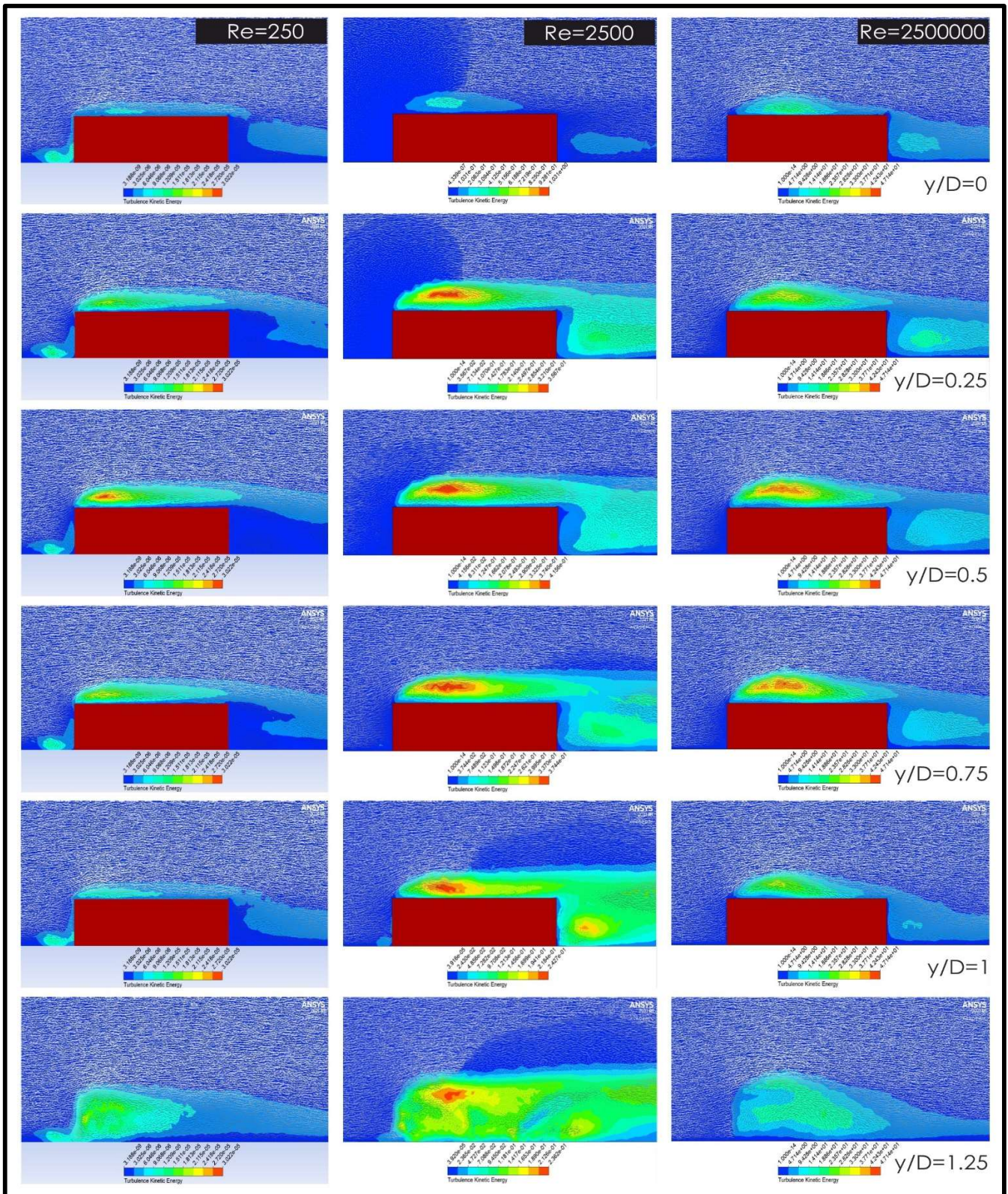


Figure 6.
Side view of Turbulence Kinetic Energy around the square prism for $y/D=0, 0.25, 0.5, 0.75, 1$ and 1.25

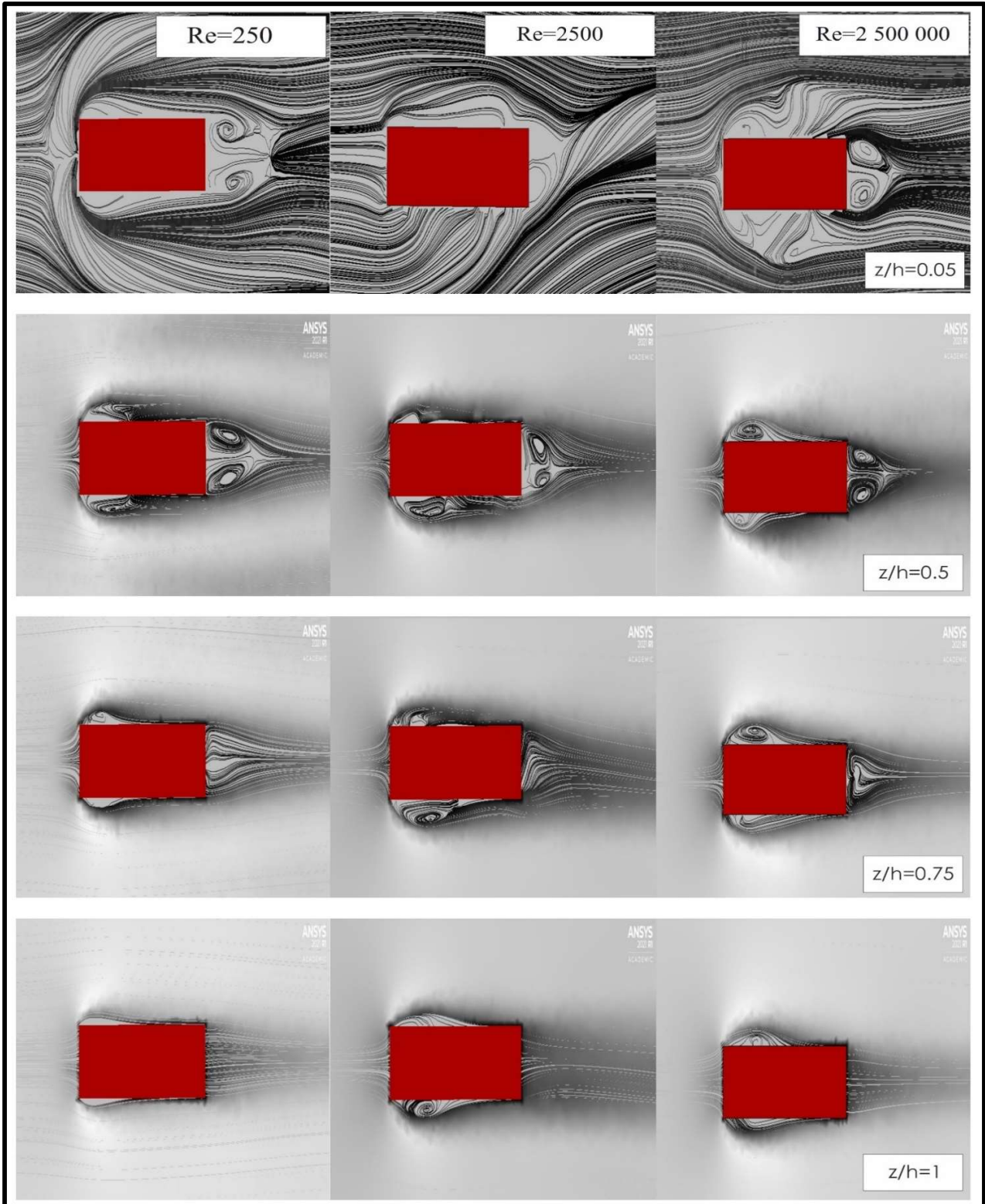


Figure 7.

Top view of the streamline passing through the square prism for $z/h=0.05$, 0.5 , 0.75 and 1

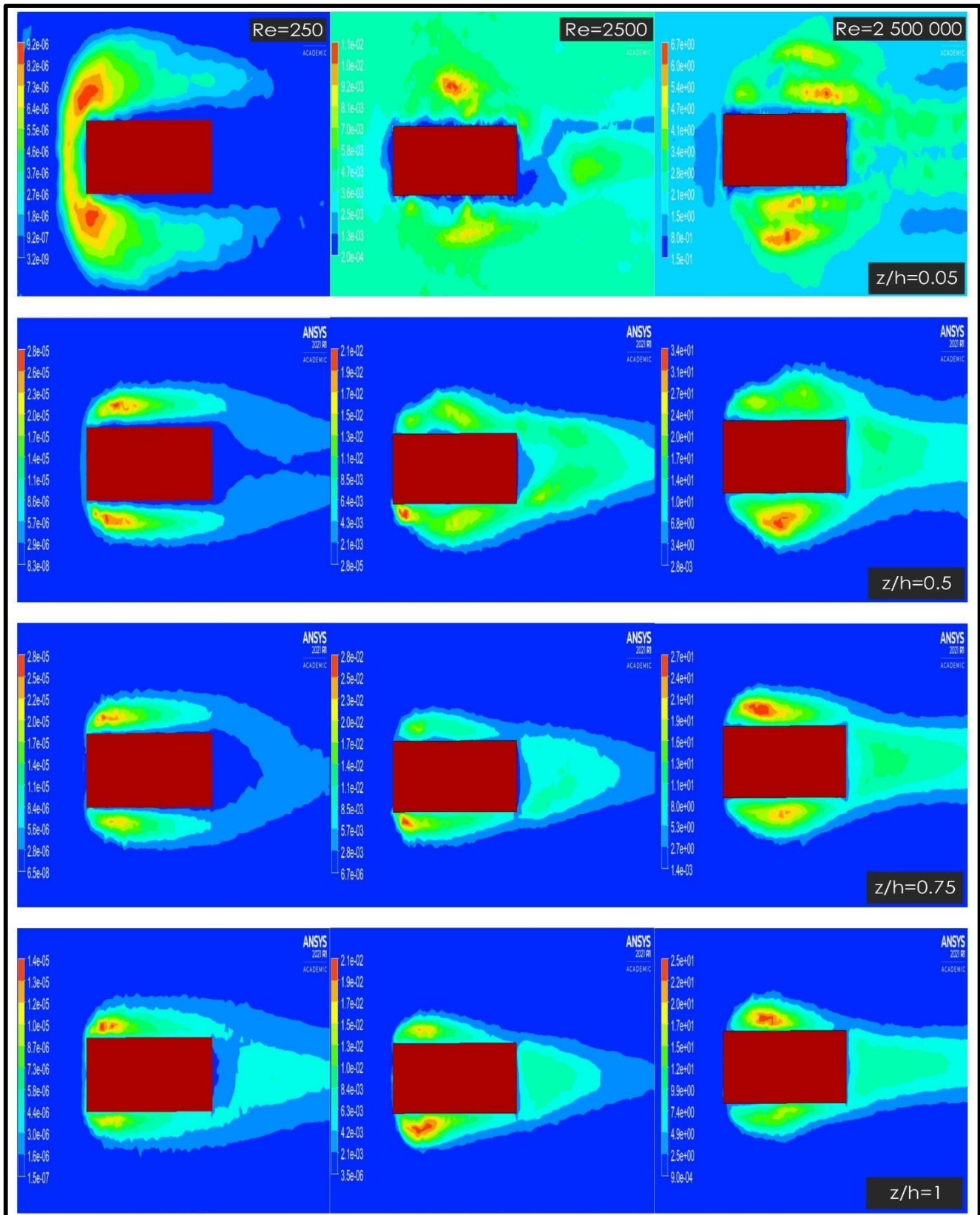


Figure 8.
Turbulent Kinetic Energy top view passing through the square prism for $z/h=0.05, 0.5, 0.75$ and 1

Conclusions

In this study, the flow structure over a ground surface-mounted square prism is numerically investigated using Ansys Fluent program. The ground surface mounted square prism model is $D=2\text{m}$ wide and 8m long with the $DR=4$. Three different Reynolds numbers ($Re=250$, $Re=2500$, $Re=2.5 \times 10^6$) are considered in this study.

It is seen that the flow in the front region of the ground surface mounted square prism forms one negative rotating vortex at the junction regions of the ground surface mounted square prism and the plane plate and this negative vortex is more stable for $Re=250$ and becomes unstable as the Reynolds number increases.

When the flow on the ground surface mounted square prism free surface was analyzed, a separation bubble was observed at the trailing edge of the ground surface mounted square prism free surface at a distance of $y/D=0.5$ for $Re=250$. It is observed that the size of the separation bubble increases as the Reynolds number increases. For Reynolds numbers $Re = 250$, 2500 and 2.5×10^6 , the separation bubble sizes formed on the ground surface mounted square prism were measured as $1.04D$, $2.01D$ and $2.26D$, respectively. The flows behind the ground surface-mounted square prism reveal a complex three-dimensional structure that is affected by the horseshoe vortex structure at the base, vortex ruptures in the center region of the ground surface-mounted square prism, and flow structures on the free surface.

When the flow in the back region of the square prism mounted on the ground surface is examined, a saddle point is formed at the base of the flow region. The saddle point divides the flow into two, towards the free end of the square prism and towards the ground plane. It is seen that the saddle point distances decrease with increasing Reynolds number.

As a result, it is seen that the flow on the ground surface mounted square prism is a combination of many vortex systems and has a complex nonpermanent structure. In the back region of the ground surface mounted square prism, it is observed that a complex flow structure is formed downward from the free surface of the square prism. It was determined that the effect of the square prism the Depth Ratio ($DR=4$) on the formation of this complex structure was high. When evaluated in terms of engineering applications, it is thought that the complex flow structure may create undesirable situations such as structural problems.

Peer-review: Externally peer-reviewed

Author contributions:

O.K : Writing, Literature Search, Analysis

C.K : Supervision, Conceptualization

Financial disclosure: This research received no external funding.

Conflict of Interest: The author has no conflicts of interest to declare.

References

Ansys Fluent Theory Guide 49-50 pp.

Chen, J., & Wu, J. (2024). Numerical investigation of vortex-induced vibration of a porous-coated cylinder at subcritical Reynolds number with a combined $k-\epsilon$ model for porous medium. *Ocean Engineering*, 304, 117828.

Durhasan, T. (2020). Flow topology downstream of the hollow square cylinder with slots. *Ocean Engineering*, 209, 107518.

Gao, Y., & Chow, W. K. (2005). Numerical studies on air flow around a cube. *Journal of Wind Engineering and Industrial Aerodynamics*, 93(2), 115-135.

Goswami, S., & Hemmati, A. (2023). Mean wake evolution behind low aspect-ratio wall-mounted finite prisms. *International Journal of Heat and Fluid Flow*, 104, 109237.

Kawai, H., Okuda, Y., & Ohashi, M. (2012). Near wake structure behind a 3D square prism with the aspect ratio of 2.7 in a shallow boundary layer flow. *Journal Of Wind Engineering And Industrial Aerodynamics*, 104, 196-202.

Korukçu, M. Ö. (2020). Kare silindir üzerinden laminar sürekli akışta blokaj oranının ısı transferi ve akış karakteristiklerine etkisinin sayısal olarak incelenmesi. *Uludağ Üniversitesi Mühendislik Fakültesi Dergisi*, 25(1), 379-390.

Kucukkurt, O., & Karakus, C. (2024). *Zemin yüzeye monteli küp üzerindeki akış yapısının sayısal olarak incelenmesi*. AHI EVRAN International Congress on Scientific Research – IV, 578-590.

Liu R. (2019). Flow around with corner modification cross-sections, be power engineering of aircraft, [Master of thesis Nanjing University of Aeronautics and Astronautics, China].

Modesti, D. (2020). A priori tests of eddy viscosity models in square duct flow. *Theoretical and Computational Fluid Dynamics*, 34(5), 713-734.

Özmen, Y., & Kaydok, T. (2014). Kare kesitli bir yüksek bina üzerindeki türbülanslı akışın sayısal olarak incelenmesi. *Kahramanmaraş Sutcu Imam University Journal of Engineering Sciences*, 17(2), 15-25.

Peyvandi, E. (2024). Numerical study of condensation and conjugated heat transfer from flow in a heat exchanger. [Master of thesis Chalmers University of Technology].

Polat, C., Saydam, D. B., Söyler, M., & Özalp, C. (2022). Farklı en boy oranlarına sahip karesel prizmatik cisimler etrafındaki akış

yapısının deneysel olarak incelenmesi. *Düzce Üniversitesi Bilim ve Teknoloji Dergisi*, 10(4), 1949-1959.

Rusdin, A. (2017). Computation of turbulent flow around a square block with standard and modified k- ϵ turbulence models. *International Journal of Automotive and Mechanical Engineering*, 14(1), 3938-3953.

Shaheed, R., Mohammadian, A., & Kheirkhah, Gildeh, H. (2019). A comparison of standard k- ϵ and realizable k- ϵ turbulence models in curved and confluent channels. *Environmental Fluid Mechanics*, 19, 543-568.

Tauqeer, M. A., Li, Z., & Ong, M. C. (2017). Numerical simulation of flow around different wall-mounted structures. *Ships and Offshore Structures*, 12(8), 1109-1116.

Yüce, B. E., & Pulat, E. (2017). *Bir ofis odasındaki termal akışın kış şartlarında sayısal olarak incelenmesi*. Teskon 2017 / Isıl Konfor Sempozyumu. 2017/080

Zargar, A. (2020). Characterization of the wake of large depth-ratio cylinders at low Reynolds numbers. [Department of Mechanical Engineering University Of Alberta Master of Science Thesis].

Zargar, A., Tarokh, A., & Hemmati, A. (2021). The steady wake of a wall-mounted rectangular prism with a large-depth-ratio at low Reynolds numbers. *Energies*, 14(12), 3579.

Zerrin, S. (2021). Kare silindir etrafında akış ve tümlleşik taşınım ile ısı geçişi. *Karaelmas Fen ve Mühendislik Dergisi*, 11(2), 145-153.

Wang, F., & Lam, K. M. (2021). Experimental and numerical investigation of turbulent wake flow around wall-mounted square cylinder of aspect ratio 2. *Experimental Thermal and Fluid Science*, 123, 11032



Climate and Energy Analysis for Erzurum

Erzurum için İklim ve Enerji Analizi

Zeynel Abidin BABA

Atatürk University, Institute of Science, Department of Mechanical Engineering. Erzurum, Türkiye .



Gökhan ÖMEROĞLU

Atatürk University, Faculty of Engineering, Mechanical Engineering, Thermodynamics Department Erzurum, Türkiye.



ABSTRACT

With the technological developments and the increase in population day by day, the need for energy has become greater than before, and this has led to the need to study energy. It is seen that energy consumption and energy use will increase day by day. In the face of this situation, it is important for researchers to work on climate and energy analysis. Within the scope of the study, the degree-day values to be used in calculating the amount of energy required to meet the heating and cooling needs for Erzurum province will be calculated.

This study was carried out using degree-day methods, which are among the building energy analysis methods. The results were obtained by using the heating degree-day and cooling degree-day methods separately within the degree-day methods.

The data obtained within the scope of the study were obtained from the General Directorate of State Meteorological Affairs, and Erzurum province was analysed in terms of temperature, relative humidity, wind, rain, frost, sun, and climate.

As a result of the necessary analyses, it has been determined that the heating need of Erzurum province is felt on most days of the year, and a large part of the energy consumption is used by heating systems. It has been determined that the cooling need is very low in Erzurum province, and it has been determined as a result of the analyses that cooling systems can be operated in an insignificant part of the year.

Keywords: Erzurum, Climate, Energy Analysis, Wind, Solar

ÖZ

Teknolojik gelişmeler ve nüfusun her geçen gün artmasıyla birlikte enerjiye olan ihtiyaç eskisinden daha fazla hale gelmiş, bu da enerji konusunda çalışma yapılması ihtiyacını doğurmuştur. Enerji tüketiminin ve enerji kullanımının her geçen gün artacağı görülmektedir. Bu durum karşısında araştırmacıların iklim ve enerji analizleri üzerine çalışmaları önem arz etmektedir. Çalışma kapsamında Erzurum ili için ısıtma ve soğutma ihtiyacının karşılanması için gerekli enerji miktarının hesaplanmasında kullanılacak derece-gün değerleri hesaplanacaktır.

Bu çalışma, bina enerji analiz yöntemleri arasında yer alan derece-gün yöntemleri kullanılarak gerçekleştirilmiştir. Derece-gün yöntemleri içerisinde ısıtma derece-gün ve soğutma derece-gün yöntemleri ayrı ayrı kullanılarak sonuçlar elde edilmiştir.

Çalışma kapsamında elde edilen veriler Devlet Meteoroloji İşleri Genel Müdürlüğü'nden temin edilmiş olup, Erzurum ili sıcaklık, bağıl nem, rüzgâr, yağmur, don, güneş ve iklim yönünden analiz edilmiştir.



Received/Geliş Tarihi : 29.01.2024
Accepted/Kabul Tarihi : 14.04.2024
Publication Date/Yayın Tarihi : 30.06.2024

Corresponding Author/Sorumlu Yazar:
Zeynel Abidin BABA
E-mail: zeynelabidin02@gmail.com

Cite this article: Baba, Z.A., Ömeroglu G., (2024).
Climate And Energy Analysis for Erzurum.
Journal of Energy Trends, 1(1), 33-42.



Content of this journal is licensed under a
Creative Commons Attribution-Noncommercial
4.0 International License.

Gerekli analizler sonucunda Erzurum ilinin ısıtma ihtiyacının yılın çoğu gününde hissedildiği ve enerji tüketiminin büyük bir kısmının ısıtma sistemleri tarafından kullanıldığı tespit edilmiştir. Erzurum ilinde soğutma ihtiyacının çok düşük olduğu tespit edilmiş olup, yılın önemsiz bir bölümünde soğutma sistemlerinin çalıştırılabileceği analizler sonucunda belirlenmiştir.

Anahtar kelimeler: Erzurum, İklim, Enerji Analizi, Rüzgâr, Güneş

Introduction

With the development of industry around the world, energy demand and consumption are increasing. With the development of factories within the scope of industry, the excessive consumption of electronic tools and equipment, and the introduction of electric cars, which appeal to a significant area of our lives today, it has become inevitable that energy has become the most basic need. As a result of developments in the industrial field, it shows that the quality of welfare in daily life is related to industrialization. With the increasing interest in technological tools in human life and the expansion of the usage area, the need for energy is increasing day by day. Individual energy consumption also shows a visible increase in the world and in our country. With these increases, providing economical and reliable access to energy worldwide can be stated as the most basic desire. With these developments, energy consumption is constantly increasing worldwide.

The amount of energy consumed from the beginning of industrialization until today creates the impression that fossil fuels will run out in the near future. In line with the studies conducted, it is seen that energy consumption worldwide is faster than the formation of fossil fuels. With the decrease in fossil fuels, the need for alternative energy sources has become an important situation. In line with these impressions, the use of energy sources other than fossil fuels should be increased. Solar energy, wind energy, etc. In line with the widespread use of renewable energy sources, this expectation has begun to be included in daily life.

Energy Analysis

The process of determining the energy in a system by checking the input and output values is called energy analysis. There is a high amount of energy consumption in industrial facilities or residences. Energy analysis can be performed on devices in industrial or residential buildings and on residential heating and cooling systems. As a result of energy analysis, input and output energy is taken under control, efficient use of energy is aimed and energy savings are achieved. At the same time, as a result of energy analysis applications, it can be observed how much of the energy entering the system is expelled without being used. As a result of the analysis, areas for improvement and development can be identified (Üçüncü, K., 2016).

Institutional Foundations

Analyses using the degree-day method have been continuing since 1928. Kennard et al. (2022) examined in their study how the degree-day method has been used in the last forty years. In their studies, they stated that degree-day change is due to global population growth and climate change. In their study, Nazan et al. (2018) examined how heating and cooling day temperatures may change as a result of climate change in Turkey. They compared the predicted future heating and cooling day temperatures with historical data. As a result of this comparison, they concluded that there would be a decrease in heating degree-days (HDDs) and an increase in cooling degree-days (CDDs). As a result of the study, it was concluded that HDDs will decrease the most in the upcoming period in Kayseri, Sivas, Mersin, and Kahramanmaraş provinces. In his study, Aslan (2022) examined the change in heating and cooling degree hours (HDH and CDH) at different equilibrium temperatures for Bandırma. In his study, he calculated HDH and CDH values for 21 years of Bandırma data by considering three different equilibrium temperatures. As a result of his study and 21 years of data, he concluded that the outdoor temperature is gradually increasing. (Erdoğan & Yılmaz, 2012) included information about building energy analysis methods in their study. This study includes detailed information about energy analysis methods.

They explained the necessary data about the types and classifications of building energy analyses and how they can be applied. Particularly, degree-day methods and bin methods were emphasized, and all necessary equations were mentioned. In their publication on building energy analysis, Erdoğan and Yılmaz (2012) examined and conveyed the necessary topics about the analysis methods that should be carried out and maintained in order to protect energy resources. They stated why building energy analyses are needed, the factors affecting the energy used in buildings, and the methods required for the selection of building energy analyses. Kayın (2019) carried out the energy performance analysis of the annex building of Namık Kemal University Çorlu Engineering Faculty. As a result of the study, a significant reduction in energy consumption was achieved with the inclusion of renewable energy sources into the system. (Bayraktar, 2003) revealed the degree-day values of station number 2218, which is affiliated with DMI General Directorate, as a result of analysis. He completed degree-day

calculations with specific outdoor and indoor temperatures between 1978 and 1998. Baumert and Selman (2003) calculated HDDs and CDDs for 171 countries. As a result of this calculation, the heating and cooling amounts that should be used per person in the countries were determined.

In their study, Büyükalaca et al. (2001) determined heating and CDDs across Turkey using degree-day methods. They used five different base temperatures in their studies. For the HDD calculation, the base temperature was determined as 22°C, and in the CDD calculation, six different values between 18° and 28°C were used as the base temperature. Calculations for all provinces in Turkey have been completed and tabulated. Bulut (2001) created detailed climate data for Adana province. They determined HDD and CDD values by taking into account different equilibrium point temperatures. They made their calculations by determining 8-hour periods for the bin method, which is among the energy analysis methods.

Heating Degree Days (HDD)

Certain comfort conditions are required in buildings. In order to prevent these comfort conditions from deteriorating, the ambient temperature must not fall below the determined base temperature value. If the ambient temperature falls below the specified base temperature, the environment must be heated in order to prevent the comfort structure from deteriorating. Using HDD data, the amount of energy required to heat the environment is determined (Akbulut, 2019).

Measured daily average temperatures provide certain results about the heating needs of buildings and the amount of energy required for this heating process. While designing and analyzing the building, it should be known how the building behaves in the winter conditions of the region where it is built, so that the heating process can be carried out correctly and with energy efficiency. It is important to know the necessary data about winter conditions before building design and construction, as heating systems must operate in all kinds of difficult conditions (Gültekin, 1995). Monthly HDD Values for 18.3°C Base Temperature between 1970-2020 are given in Table 1.

Cooling Degree Days (CDD)

CDDs, unlike HDDs, are used to determine the amount of energy required to cool and ventilate the environment in order to increase human comfort in hot weather. Necessary cooling equipment and electronic systems are used to cool the environments inside buildings. CDD methods are preferred in order to determine the amount of energy consumed by cooling systems and to increase energy efficiency.

The base temperature value, which is among the parameters required to calculate the CDD index, is accepted as 24°C. This parameter is also used throughout Türkiye. In summer, cooling

and ventilation needs increase as the outdoor temperature exceeds 24°C due to hot weather. When the temperature exceeds the specified value, CDDs can be calculated by subtracting the base temperature from the average outdoor temperature value. For example, on a day when the average outdoor temperature is 25°C, the base temperature, which is accepted as 24°C, is subtracted from this value, and the CDD value is stated as 1°C (Gültekin, 1995). Table 1 shows the values related to HDD.

Steady State Methods

The energy analysis method, which is another form of building energy analysis method, is divided into two separate groups depending on whether it is continuous or not. These two groups are called steady-state methods and dynamic methods. Less data is needed in analyses performed with steady-state methods. It is preferred in simple applications. Under this heading, types of steady state methods will be explained. The bin method, the data-based bin method, and the correlation method will be introduced.

Bin Method

While energy analysis is carried out using the Bin method, energy consumption is analyzed on a monthly and annual basis by evaluating time and temperature ranges. Bin values used in the bin method are defined as the number of hours during which temperature ranges are observed within a time period. The Bin method does not depend on daily average outdoor temperature values, as in other methods. Instead, hourly climate values are taken into account. In this way, it provides clearer results than degree-day methods (ASHRAE, 2009; Erdoğan, et al., 2012).

Adjusted Bin Method

Maximum loads are taken into account when using the bin method, which is one of the energy analysis methods. Considering the different loads, it appears to be in off-design conditions. By taking these conditions into account, more accurate load profiles are created. The basic logic of the corrected bin method also depends on these parameters (Erdoğan & Yılmaz, 2012).

8760 Hourly Method

In the 8760 hourly method, 8760 hourly calculations are made for each day of the year, taking into account the outdoor temperatures when the residences and systems operate. With this energy analysis method, the amount of annual energy consumption can be determined clearly by performing analyses for all days and hours. At the same time, it is seen that situations that cannot be determined clearly in other analysis methods or that make calculations difficult are eliminated with this method. The reason for this may be the use of clear weather data for each

hour. In addition, when performing energy analysis, the number of people in the building or workplace, the lighting used, hourly and daily usage data of heating and cooling systems, and the energy consumption of the equipment used to increase human comfort are also included in these calculations. The clearest data for determining the amount of energy used can be easily obtained for 8760 hours thanks to this method (Alarko, 2007).

Material and Methods

Erzurum is among the cities located in the Eastern Anatolia Region, with high altitudes and continental climate characteristics. Some districts in Erzurum do not show the same climate characteristics as the center. Oltu, Olur, Tortum, Uzundere, and İspir districts are affected by the Black Sea Region in terms of their climate characteristics due to their proximity to the Black Sea Region. It is known that continental climate conditions are observed in the villages or neighborhoods of the mentioned districts with high altitude values.

When the data received from the General Directorate of Meteorology for the energy analysis of Erzurum province is examined, it is seen that the number of frosty days with monthly temperature values of -0.1°C and below between 1970 and 2020 was highest in December, January, and February. The months with the least number of frosty days are naturally stated as the months in which the summer season occurs. Frosty days, which occur rarely in June, July, and August, were evaluated with the help of data obtained from areas with high altitude.

When the annual rainfall amounts of Erzurum province are examined, the months with the most rainfall are April and May. According to the data, there is an average annual rainfall of 412.2 mm. The month with the least rainfall was determined to be August. In the period from 1970 to 2020, the year with the most rainfall was 2015, and the amount of rainfall was 593.3 mm.

According to annual data for Erzurum, the coldest month is January, and the hottest month is August. From here, the importance of energy analysis can be understood once again. Controlling energy consumption in January, which has an average temperature of approximately -10°C , is possible with energy analysis. HDD and CDD numbers are determined using degree-day methods, and necessary precautions can be taken by taking these numbers into consideration. HDD and CDD numbers are determined based on average temperatures.

Winds are most intense in April, May, and July. The average wind speed in these months was determined to be 3.35 msec^{-1} , 3.19 msec^{-1} and 3.5 msec^{-1} , respectively. According to the data, the months with the lowest wind speeds are December and January.

Impact of Urbanization

Climatic changes are observed in cities with the increase in human population, number of buildings, industrial construction, and energy consumption. It has been explained in the previous headings that with the increase in population, the need for energy is constantly increasing due to the materials people use to increase their living comfort. When we consider the winter season, it can be said that the need for heating is high in cities with a high population, and therefore, a certain amount of heat is transferred to the atmosphere from each house. As heat transitions occur, the air also becomes warmer. When we consider that the number of buildings increases with the population, the warming of the weather cannot be ignored.

As a result of the increase in production along with the development of industry and technology, energy consumption and the temperature created by gases transferred to the environment increase. The gases released into the environment as a result of the fuels used by public transportation vehicles or individual vehicles also increase this value.

Erzurum Province Heating and Cooling Degree Day Values

Within the scope of the thesis study, heating and CDD values were determined for Erzurum province. Average temperature values between 1970-2020 were obtained from MGM (Meteoroloji Genel Müdürlüğü). Degree-day values were created using average temperature values, HDD and CDD equations. The equations in formula 1 and formula 2 below were used when making the calculations.

HDD: Heating Degree Days,

CDD: Cooling-degree-day.

n : Number of Days in Period,

T_t : Base Temperature,

T_{ort} : Daily Average Outdoor Temperature.

$$\text{HDD} = \sum_1^n [T_t - T_{ort}] \quad (1)$$

Formula 1.

Heating-degree-day calculation equation.

$$\text{CDD} = \sum_1^n [T_{ort} - T_t] \quad (2)$$

Formula 2.

Cooling-degree-day calculation equation.

HDD values are given in monthly periods in the Table 1 created at five-year intervals since 1970. Considering the base temperature of 18.3°C throughout most of the year, it has been observed that the need for heating occurs. The need for heating begins in autumn and continues until the end of spring. Due to the climate structure of Erzurum, the need for heating is felt in the summer months. When the data is examined day by day, the days when heating is needed cover most of the year.

It is known that cooling needs occur at temperatures of 24°C and above. When this value was taken into account as the base temperature and the necessary calculations were made and evaluated over five-year periods, the data in Table 2 was

obtained. According to the data, it can be seen that the need for cooling is not felt much in Erzurum.

Table 1.
Monthly HDD Values Between 1970-2020 for Base Temperature 18.3°C

Range Of Years	Jan	Feb	Mar	Apr	May	Jun	Jul	Aug	Sep	Oct	Nov	Dec	Annual Average	Total Days Required For Heating
1970 - 1974	886.56	722.40	592.46	375.60	239.84	123.62	24.70	36.38	105.98	288.30	550.54	801.06	395.62	1611.00
1975 - 1979	827.22	680.88	615.38	376.4	252.24	120.04	33.48	15.34	99.06	335.52	490.04	728.96	381.21	1578.00
1980 - 1984	821.18	735.48	604.5	395.6	271.96	110.32	19.42	33.98	104.1	315.38	506.36	704.32	385.22	1589.00
1985 - 1989	841.92	745.64	671.6	368.14	241.86	112.16	22.64	24.42	132.64	351.42	572.92	771.42	404.73	1591.00
1990 - 1994	955.76	859.28	723.68	391.58	267.62	131.28	31.08	21.38	132.1	320.96	597.52	827.30	438.30	1638.00
1995 - 1999	818.84	774.86	696.34	418.94	227.5	115.76	27.06	15.68	163.42	348.46	533.18	745.62	407.14	1619.00
2000 - 2004	909.38	764.22	646.24	390.34	266.42	120.34	20.28	29.2	132.62	323.66	559.16	839.28	416.76	1622.00
2005 - 2009	980.70	770.32	586.04	386.02	237.98	106.04	24.24	18.38	127.52	309.84	525.18	768.80	403.42	1593.00
2010 - 2014	822.50	737.06	590.16	354.66	228.88	92.48	16.82	5.88	109.64	320.64	533.16	775.02	382.24	1557.00
2015 - 2020	850.43	724.67	554.17	374.52	229.40	86.03	9.03	7.82	88.32	294.08	526.87	756.97	375.19	1827.00

* The sum of the temperature differences that will meet the daily heating requirement required to reach 18.30°C.

Table 2.
Monthly CDD Values Between 1970-2020 for a Base Temperature of 24°C

Range Of Years	Jan	Feb	Mar	Apr	May	Jun	Jul	Aug	Sep	Oct	Nov	Dec	Annual Average	Total Days Required For Cooling
1970 - 1974	0.00	0.00	0.00	0.00	0.00	0.00	0.50	0.72	0.00	0.00	0.00	0.00	0.10	8.00
1975 - 1979	0.00	0.00	0.00	0.00	0.00	0.00	0.74	0.40	0.00	0.00	0.00	0.00	0.10	9.00
1980 - 1984	0.00	0.00	0.00	0.00	0.00	0.00	2.18	0.22	0.00	0.00	0.00	0.00	0.20	19.00
1985 - 1989	0.00	0.00	0.00	0.00	0.00	0.00	0.10	0.54	0.00	0.00	0.00	0.00	0.05	9.00
1990 - 1994	0.00	0.00	0.00	0.00	0.00	0.00	0.64	0.00	0.00	0.00	0.00	0.00	0.05	4.00
1995 - 1999	0.00	0.00	0.00	0.00	0.00	0.00	0.06	0.06	0.00	0.00	0.00	0.00	0.01	2.00
2000 - 2004	0.00	0.00	0.00	0.00	0.00	0.00	1.38	0.86	0.00	0.00	0.00	0.00	0.19	12.00
2005 - 2009	0.00	0.00	0.00	0.00	0.00	0.00	0.14	3.96	0.00	0.00	0.00	0.00	0.34	13.00
2010 - 2014	0.00	0.00	0.00	0.00	0.00	0.00	0.50	0.34	0.00	0.00	0.00	0.00	0.07	8.00
2015 - 2020	0.00	0.00	0.00	0.00	0.00	0.00	0.43	1.12	0.00	0.00	0.00	0.00	0.13	11.00

* The sum of the temperature differences that will meet the daily cooling need required to reduce 24°C.

Research Findings

Within the scope of the thesis study, in light of the data obtained from the General Directorate of Meteorology for Erzurum province between 1970 and 2020, monthly numbers of frost days, average current pressure values, average relative humidity values, average wind speeds, average temperatures, total sunshine durations, total rainfall amounts, and average soil temperatures were examined. As a result of these examinations, HDDs and CDDs in the degree-day method were evaluated, and the necessary analyses were made. Necessary interpretations

regarding Erzurum climate and building energy analyses were made by examining the analysis tables.

When the winter and summer seasons in Erzurum are examined, it can be said that most of the year is under the influence of the winter season. It is known that snowfall and icing increase in December, January, and February, when air temperatures are at their lowest values, and the harshest winter conditions are experienced in these months. The highest number of frosty days was determined in the winter of 1992. 207 days of the year were announced as frost days, and all days of December and January were determined as frost days.

When the sunshine duration of the province was examined using 51 years of data, it was determined that the highest sunshine duration was in 2017 with 2870 hours annually, taking into account the deficiencies of the 2009-2011 data. When evaluated monthly, it is seen that July has the highest sunshine duration. The total amount of precipitation was determined to be 412.2 mm on average annually, based on data received from MGM.

Monthly Numbers of Frosty Days in Erzurum Province

The number of frost days in Erzurum province was examined with data from MGM between 1970 and 2020. Erzurum is one of the provinces that has a continental climate and spends most of the year under the influence of winter. Frost events occur due to harsh winter conditions. Frost events occur when the air temperature is -0.1°C or below. Based on the data examined since 1970, it is known that the highest number of frosty days belongs to 1992, with 207 days. The least number of frosty days belongs to 1979, with 135 days. Average, minimum and maximum values of the number of frosty days by month between 1970-2020 are given in Table 3.

Table 3.

Average, Minimum and Maximum Values of the Number of Frosty Days Between 1970 and 2020 by Month

Month/Value	Average Number of Frosty Days	Minimum Number of Frosty Days	Maximum Number of Frosty Days
January	30.6	28	31
February	27.6	24	29
March	26.7	15	31
April	13.8	2	24
May	2.8	1	11
June	0.37	1	3
July	1	1	1
August	1	1	1
September	2.1	1	9
October	12.1	1	27
November	23.5	11	30
December	29.3	22	31

Total Monthly Sunshine Time in Erzurum Province

Monthly average sunshine durations across Erzurum were determined with the data between 1970 and 2020 obtained from MGM. Although Erzurum province has harsh winter conditions, it has a certain amount of sunshine every month of the year. The months with the highest amount of sunshine were observed in

June, July, and August. When we look at the months with the least solar energy, it is seen that December, January, and February receive less solar energy on average. As a result of examining 51 years of data, the maximum total sunshine duration was recorded as 392.4 hours in July 1971.

Average, Minimum and Maximum Values of Total Sunshine Times by Month between 1970-2020 are given in Table 4

Table 4.

Average, Minimum and Maximum Values of Total Sunshine Times by Month between 1970-2020

Month/Value	Monthly Average Sunshine Time (Hours)	Minimum Average Sunshine Time (Hours)	Maximum Average Sunshine Time (Hours)
January	97.15	43	187
February	118.16	65.7	215.2
March	154.8	94.9	252.1
April	181.4	124.6	285.7
May	235.45	154.9	306.8
June	293.22	258.7	357.2
July	341.48	249	392.4
August	326.7	250.1	379.5
September	266.5	213.2	316.8
October	204.36	144.5	273.5
November	135.6	71.2	210.9
December	89.95	27.8	181.9

Erzurum Province Monthly Total Precipitation

Taking into account the data between 1970 and 2020, the average monthly rainfall amounts for 51 years were calculated. In addition, the minimum and maximum precipitation values for each month are determined and shown in the chart. The highest average rainfall occurs in May. When the data are examined separately for each year, the amount of precipitation gradually increases from January to June and then begins to decrease. The months with the least rainfall are December, January, February, and August. As a result of examining the 51-year data taken into account in the analysis with average values, August is stated to be the month with the least rainfall among other months. Monthly Average, Minimum and Maximum Rainfall Amounts with 1970-2020 MGM Data are given in Table 5.

Erzurum Province Monthly Average Temperature

The lowest average daily temperature recorded in MGM between 1970 and 2020 in Erzurum was determined to be -29.6°C. The highest daily average temperature was recorded to be 28.20 °C. When the data received from MGM was examined, it was determined that the highest monthly average temperature belonged to August, and the lowest monthly average temperature belonged to January with -16.9. In this thesis study, building energy analysis will be carried out using the degree-day method, using daily average temperature values. Monthly General, Minimum and Maximum Temperature Averages According to 1970-2020 MGM Data are given in Table 6.

Erzurum Province Monthly Average Wind Speed

Wind speeds recorded between 1970 and 2020 were examined together with the data received from MGM for Erzurum province. The month with the highest wind speed is July, with an average of 3.43 msec⁻¹. Within the data, the lowest monthly wind speed belongs to November, with 0.2 msec⁻¹. The highest average wind speed occurred in October at 5 msec⁻¹. As a result of 51 years of investigation, the lowest wind speed was determined to be November 1994. The highest wind speed was recorded in 1987. When the wind direction, which is constantly dominant in Erzurum, is examined, western (W) winds are effective throughout the province (Karaca et al., 2013). Monthly General, Minimum, Maximum Wind Speed Averages and Wind Directions According to 1970-2020 MGM Data are given in Table 7.

Table 5.

Monthly Average, Minimum and Maximum Precipitation Amounts with 1970-2020 MGM Data

Month/Value	Monthly Average Precipitation Amount (mm)	Minimum Average Monthly Precipitation Amount (mm)	Maximum Average Monthly Precipitation (mm)
January	18.7	1.7	55.7
February	22.01	1.2	90
March	30.8	1.2	82.2
April	55.3	8.8	150.2
May	70.3	14.9	154
June	44.4	2.9	112.6
July	24.65	0.8	92.6
August	17.52	0	63
September	21.7	0	76.2
October	47.3	2.3	210.8
November	30.7	1.6	81
December	21.07	4.9	52.8

Table 6.

Monthly General, Minimum and Maximum Temperature Averages According to 1970-2020 MGM Data

Month/Value	Monthly Average Temperature (°C)	Minimum Monthly Average Temperature (°C)	Maximum Monthly Average Temperature (°C)
January	-9.8	-16.9	-3.9
February	-8.26	-15.1	-1.9
March	-1.91	-10.4	4.6
April	5.53	1.4	9
May	10.36	7.5	12.6
June	14.72	12.6	17.8
July	19.14	16.8	22.2
August	19.32	16.6	22.7
September	14.5	11.6	17.6
October	7.95	5.1	11.9
November	0.32	-5.6	4.5
December	-6.59	-14.2	-0.8

Table 7.

Monthly General, Minimum, Maximum Wind Speed Averages and Wind Directions According to 1970-2020 MGM Data

Month/Value	Monthly Average Wind Speed (msec ⁻¹)	Minimum Average Monthly Wind Speed (msec ⁻¹)	Maximum Average Monthly Wind Speed (msec ⁻¹) - Direction	Wind direction
January	1.87	0.4	3.3 - E	SS-W
February	2.21	0.6	3.7 - W	W
March	2.82	0.3	4.2 - WSW	W
April	3.28	0.8	4.2 - WSW	WSW
May	3.13	1.1	4.2 - SSW	WSW
June	2.95	0.5	3.9 - W	E
July	3.43	0.7	4.5 - ESE	ENE
August	3.27	0.9	4.6 - WSW	E
September	2.78	0.5	3.9 - SSW	ENE
October	2.53	0.6	5 - S	WSW
November	2.23	0.2	3.4 - W	WSW
December	2	0.4	3 - ENE	WSW

Conclusions

HDD and CDD values, which are degree-day methods, were determined by using daily average temperature data between 1970 and 2020 from the General Directorate of Meteorology for Erzurum province. Calculated degree-day values can be used to determine the amount of energy that needs to be used to meet the heating and cooling needs of Erzurum province.

In addition to monthly average degree-day values, annual average degree-day values and the number of days requiring annual heating or cooling processes were determined. In Erzurum, which has a continental climate, the need for heating is greater than cooling. The fact that winter is felt throughout most of the year also highlights this situation. The winter seasons in Erzurum are cold and snowy. When we look at the daily average temperature values obtained, it is seen that daily temperatures are generally below 0°C in winter. In these situations, it is inevitable that the need for heating will increase.

Due to harsh winter conditions throughout Erzurum province, the number of frosty days is quite high. It has been determined that frost occurs in many months of the year, except for the months of summer.

It may be possible to make industrial and technological investments in areas where the cold climate is an advantage. Storage areas can be created for natural gas. As technological investments, cooling for data centers creates a serious cost, and in this respect, data centers can be established in large areas.

Heat pump technologies are developing rapidly as thermal resources, and an alternative energy source to natural gas consumption can be offered by using deep well systems from geothermal resources. Greenhouse cultivation based on geothermal heat can be expanded for crops affected by agricultural frost.

Another analysis was carried out using the degree-day method for the province of Erzurum, and the cooling was carried out using the degree-day method. To determine the CDD values, temperature values of 18, 19, 20, 21, 22, 23, and 24°C were used as base temperatures. In human life, the need for cooling is felt at outdoor temperatures above 24°C. Average daily temperature values in Erzurum province rarely exceed 24°C at certain times of the year. This rarely encountered situation significantly eliminates the need for cooling. This means that there will be no extra energy consumption for Erzurum province. Every possibility should be taken into consideration in building designs. In this way, energy consumption can be reduced.

Peer-review: Externally peer-reviewed

Author contributions: The authors contributed equally to the research.

Financial disclosure: This research received no external funding.

Conflict of Interest: The author has no conflicts of interest to declare.

References

Akbulut, G. (2019). Climate and Energy Analysis for Ardahan Province, [Master's Thesis, Institute of Science and Technology, Atatürk University].

Alarko, (2007). 8760 Hourly Building Energy Analysis, Teknik Bülten April, 1-4 p.

An, N., Turp, M. T., Akbaş, A., Öztürk, Ö., & Kurnaz, M. L. (2018). Future Projections of Heating and Cooling Day Degrees in Turkey's Changing Climate, *Marmara Fen Bilimleri Dergisi*, 3: 227-240.

Ashrae (SI Edition), 2009. Fundamentals Handbook.

Aslan, A. (2022). Change of Heating and Cooling Degree-Hours for Different Base Temperatures: A Case Study of Bandırma. *Uluslararası Doğu Anadolu Fen Mühendislik ve Tasarım Dergisi*, 4(1), 1-14.

Baumert, K., Selman, & Mindy. (2003). Heating and Cooling Degree Days, World Resources Institute.

Bayraktar, K. G. (2003). Evaluation of Foreign Account Temperatures and Number of Degree Days for Türkiye. [Doctoral Thesis, Institute of Science and Technology, İstanbul Technical University].

Bulut, H. (2000). *Detailed Meteorological Values for Energy Analysis in Buildings in Adana Province* 6th National Cooling and Air Conditioning Technique Congress, Çukurova University, Adana.

Büyükalaca, O., Bulut, H., & Yılmaz, T. (2001). Analysis of variable-base heating and cooling degree-days for Turkey. *Applied Energy*, 69(4), 269-283.

Erdoğan, S., & Yılmaz, M. (2012). Building Energy Analysis, *Scientific, Cooling World*, Issue 15.

Erdoğan, S., Yılmaz, M., Karagöz, Ş., & Karlı, S. (2012). Steady State Building Energy Analysis Methods *Plumbing Engineering - Issue 128*.

Gültekin, M.L. (1995). Distribution of Degree-Days in Turkey. [Master's Thesis, İ.T.U. Institute of Science and Technology, İstanbul].

Karaca, A., Şenol, A., Denizli, F., Çiçek, M., & Derman, Y. (2013). Improvement of Air Quality in Cities Project Erzurum Air Quality Assessment Report.

Kayın, Ö. (2019). Binalarda enerji modellemesi, enerji performans analizi ve yenilenebilir enerji kullanımının çevre dostu yeşil bina uygulama örneği kapsamında değerlendirilmesi, [Yüksek Lisans Tezi, Namık Kemal Üniversitesi].

Kennard, H., Oreszczyn, T., Mistry, M., & Hamilton, I. (2022). Population-weighted degree-days: The global shift between heating and cooling. *Energy and Buildings*, 271, 112315.

Nazan, A. N., Turp, M. T., Akbaş, A., Öztürk, Ö., & Kurnaz, M. (2018). Türkiye'nin Değişen İkliminde Isıtma ve Soğutma Gün Derecelerinin Gelecek Projeksiyonları. *Marmara Fen Bilimleri Dergisi*, 30(3), 227-240.

Üçüncü, K. (2016). Energy Management Lecture Notes, Karadeniz Technical University Faculty of Forestry, Department of Forest Industrial Engineering.



Numerical Study of the Aerodynamic Behavior of 7.62 x 51 mm Bullet

7.62 x 51 mm Merminin Aerodinamik Davranışı Üzerine Sayısal Çalışma

Osman YAZICI



Atatürk University, Faculty of Engineering, Mechanical Engineering Erzurum, Türkiye .

Şendoğan KARAGÖZ



Atatürk University, Faculty of Engineering, Mechanical Engineering Erzurum, Türkiye.

Orhan YILDIRIM



Atatürk University, Faculty of Engineering, Mechanical Engineering Erzurum, Türkiye .

Ömer ÇOMAKLI



Atatürk University, Faculty of Engineering, Mechanical Engineering Erzurum, Türkiye .

ABSTRACT

Firearms play an important role in the defence industry. Various studies have been carried out to increase the range, destructiveness, and stabilization of these weapons. However, one of the important factors affecting these parameters is the design of the projectile core. Aerodynamic improvements in the core design can increase the range without changing the weapon design. In this study, the effect of the 7.62x39 mm bullet core on the aerodynamic flow behaviour around it was investigated. The air flow over the projectile core is analysed in the ANSYS Fluent program.

Keywords: Projectile, Projectile Core, Aerodynamics, ANSYS Fluent, Flow Field

ÖZ

Ateşli silahlar savunma sanayinde önemli bir rol oynamaktadır. Bu silahların menziline, tahrip gücünü ve stabilizasyonunu arttırmak için çeşitli çalışmalar yapılmıştır. Ancak bu parametreleri etkileyen önemli faktörlerden biri de mermi çekirdeğinin tasarımıdır. Çekirdek tasarımındaki aerodinamik iyileştirmeler, silah tasarımını değiştirmeden menzili artırabilir. Bu çalışmada, 7.62x39 mm mermi çekirdeğinin etrafındaki aerodinamik akış davranışına etki araştırılmıştır. Mermi çekirdeği üzerindeki hava akışı ANSYS Fluent programında analiz edilmiştir.

Anahtar kelimeler: Mermi, Mermi Çekirdeği, Aerodinamik, ANSYS Fluent, Akış Alanı

Introduction

In today's wars, firearms are one of the most important means of hitting the target. The bullet used in these weapons is a metallic component that is designed and fired by a mechanism within the weapon. A bullet is a whole consisting of a shell, powder, capsule, and nucleus. The nucleus of a bullet typically has no explosive effect, but when the powder in the shell is ignited by the capsule, the nucleus gains kinetic and impact energy and can damage the target. The development of efficient projectile movement is crucial for the core to reach the target. It is very important in terms of bullet damage that the exit velocity of the nucleus from the gun barrel reaches the target with minimum loss. Therefore, the velocity of the projectile depends on the flight resistance. The design parameters of the projectile are related to the drag and lift forces acting on it. The widespread use of long-range projectiles, worldwide has increased the study of the aerodynamics of projectiles and the analysis of their aerodynamic properties has become an important focus for their improvement.

Aerodynamics is the study of the mass forces of air. In the case of air flowing around a solid body or a solid body moving in still air, the air behaves in accordance with the laws of aerodynamics. In this study, the forces acting on the projectile core at supersonic speeds are analyzed using computer-based numerical analysis. In this context, a literature review was conducted, and proposals for range improvement of projectiles of different geometries supported the subject of



Received/Geliş Tarihi : 22.05.2024
Accepted/Kabul Tarihi : 17.06.2024
Publication Date/Yayın Tarihi : 30.06.2024

Corresponding Author/Sorumlu Yazar:

Osman YAZICI

E-mail: osman.yazici13@ogr.atauni.edu.tr

Cite this article: Yazici O., Karagoz S., Yildirimi O., and Comakli, O., (2024). Numerical Study of the Aerodynamic Behavior of 7.62 x 51 mm Bullet. *Journal of Energy Trends*, 1(1), 43-47



Content of this journal is licensed under a Creative Commons Attribution-Noncommercial 4.0 International License.

the study. Jovanovic et al. (2012) conducted experimental and numerical investigations to understand the hydrodynamics of flow and to model the flow around a hollow sphere and performed numerical investigations at different Reynolds numbers. In their study, they found that the RANS turbulence model gives the best results in the experimental and numerical determination of the velocity field, pressure and friction coefficient, and the length of the reverse flow region. Choi et al. (2006) investigated the flow around objects with pits, such as on a golf ball. They found that pits increase the turbulence intensity in the flow and are an important flow control strategy to reduce friction in the body. Chowdhury et al. (2016) observed that the dimpled surface on a golf ball affects the aerodynamic behavior of the ball. As a result of the study, they evaluated that the dimpled structure significantly changed the surface drag coefficient. In 1995, R.M. Cummings et al. (1995) performed numerical analysis of projectiles in supersonic turbulent flow environments and developed different designs by applying drag optimization to them. Khan and Saha (2013) investigated the aerodynamic behavior of projectile cores with different nose structures using numerical approaches and investigated the effects of velocity and pressure on sharp and rounded edge geometries. In his study, Litz (2016) examined the fluid motions acting on the projectile and stated that the narrowing geometry at the tip of the projectile reduces friction. In 1953, Murphy (1953) investigated the drag coefficient and dynamic stabilization of the projectile by performing experimental measurements on different projectile geometries. Nietubicz and Sturek (1988) conducted numerical and experimental analysis of a projectile at supersonic speed. They compared the results of experiments conducted in a wind tunnel and numerical data with the changes they made in the tail angle of the projectile. Selimli (2020), in his study, investigated the effect of the channel structure and hollow structure formed on the surface of the 9 mm parabellum type light bullet core on the aerodynamic flow behavior around the bullet. The air flow around the projectile core was analyzed with computational fluid dynamics based Fluent software. The compressible airflow is analyzed with the Spalart Allmaras turbulent flow model, taking into account the viscous effects due to Sutherland's law. In the study, he concluded that the channel or hollow surface form created by the projectile geometry can cause an increase in projectile velocity and a decrease in shear stress and drag force. He evaluated that the hollow or channel structure to be formed on the projectile surface will provide positive contributions to the range as well as stabilization in the projectile movement. In 2023, Salunke et al. (2023) examined three bullets of different diameters used in different types of weapons. The first bullet is the NATO 5.56 mm, the second is the 7.62 mm bullet from the APM2 and the third is the 7.82 mm bullet from the AK-47 rifle. For the 2D

stationary calculations, the supersonic speed of Mach 2 was adopted to analyze the flow field of all three projectiles. He observed that the 7.82 mm bullet is subjected to maximum buoyancy due to its larger surface area than the other two ammunitions. In 2024, Hao et al. (2024) analyzed the lift and drag coefficients of projectiles with different curves under different angles of attack. When they compared the analysis of the projectile with the logarithmic curve and the projectile with the von Karman curve, they observed that the lift force acting on the projectile with the logarithmic curve was higher.

In this study, the effect of the channel structure formed inside the 7.62x51 projectile core on the aerodynamic behavior of the projectile is evaluated. The compressible flow around the projectile core is analyzed in ANSYS Fluent software using the Spalart Allmaras turbulent flow model, which is used in aerospace and outdoor aerodynamic analysis, considering viscous effects due to Sutherland's law. By examining the flow behavior around the projectile core, the contribution of the design to range and target stabilization is investigated, and it is aimed to contribute to the related field.

Material and Methods

The 7.62-diameter bullet has a bullet diameter of 32.5-mm, a bottom diameter of 6.29-mm and a tip diameter of 1.5-mm. Two-dimensional models of the core were created in Ansys Design Modeler software. The dimensions of the bullet core are 7.62X51 mm. The created bullet core models are visualized in Figure 1.

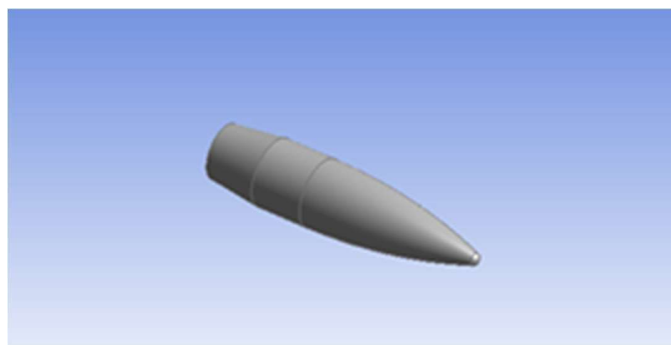


Figure 1.
Bullet core

A wind tunnel is designed around the projectile core in ANSYS program. The flow velocity at the entrance of the tunnel is assumed to be 800 ms^{-1} , the exit velocity of the projectile from the barrel is 800 ms^{-1} , the open air pressure is 101325 Pa, and the ambient temperature is 300 K. The wind tunnel is shown in Figure 2.

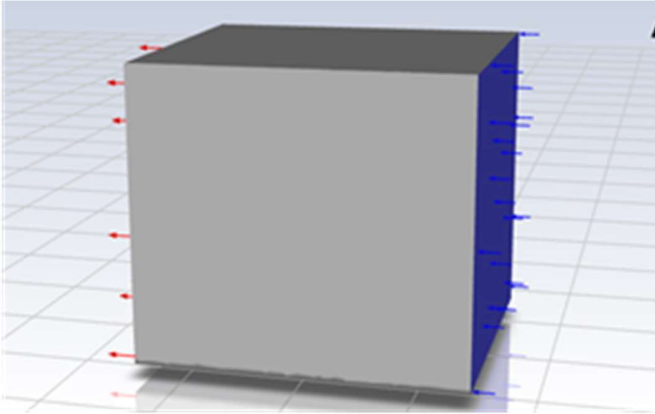


Figure 2.
Wind tunnel

In order to examine the effect of airflow around the projectile core models on aerodynamic behavior, the external flow body model mesh structure was created using Ansys Meshing software. The generated mesh model is visualized in Figure 3.

The network structure was created with 1640938 cells and an average quality of 77%. While creating the network structure, the inflation command was used for better results of pressure, velocity, and density changes in the boundary layers on the projectile.

The airflow around the projectile core was analyzed using Fluent software based on computational fluid dynamics. The compressible airflow is analyzed with the Spalart Allmaras turbulent flow model used in aerospace and outdoor aerodynamic analysis, taking into account the viscous effects due to Sutherland's law.

Convergence criteria have been identified in Fig. 4 to show the problem solving process in 500 iterations. In this figure, variations of the continuity, velocity, and energy residuals has been presented respectively.

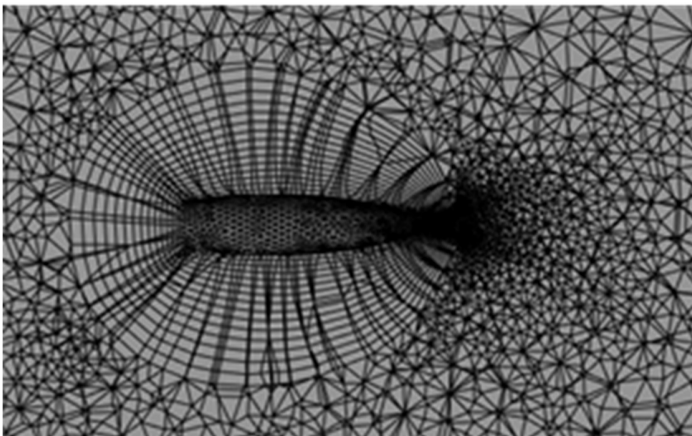


Figure 3.
Mesh model

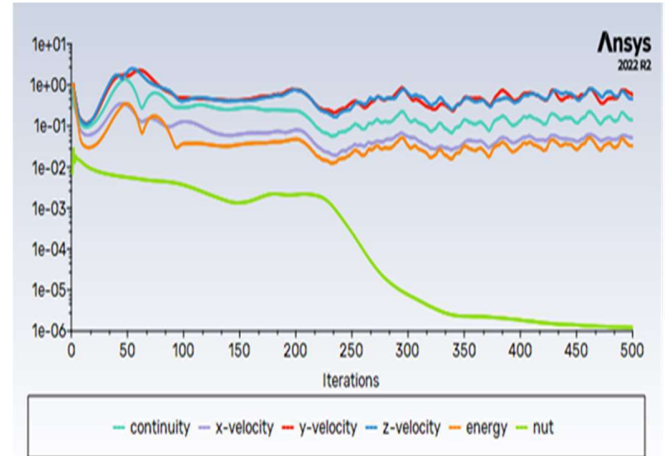


Figure 4.
Residual variations versus iteration number

Results

In this study, the aerodynamic parameters velocity, pressure, and density values obtained as a result of the analyses performed for the 7.62x51 bullet core model are analyzed. As a result of the analysis, it was observed that the flow velocity around the projectile, which has an exit velocity of 800 m s^{-1} , decreases to 44 m s^{-1} in the rear region of the projectile. The reason for this is the edginess of the projectile geometry. When the average flow velocity around the projectile core is evaluated, it is seen that there is a decrease in the flow velocity around the core and a 94.5% decrease in the rear part of the projectile. In this context, the velocity distributions around the projectile core are visualized in Figure 5 for Mach number 2.3. The results obtained here are in agreement with scientific studies (Dođru, 2017)

In an environment where the atmospheric pressure is assumed to be 101325 Pa, it is seen that the pressure increases to 130000 Pa at the tip of the projectile, while it decreases to -30000 Pa at the back of the projectile. This decrease in pressure was calculated to be 130%. The pressure distributions around the projectile core are visualized graphically in Figure 6 for Mach number 2.3. The results obtained here are in agreement with scientific studies (Dođru, 2017)

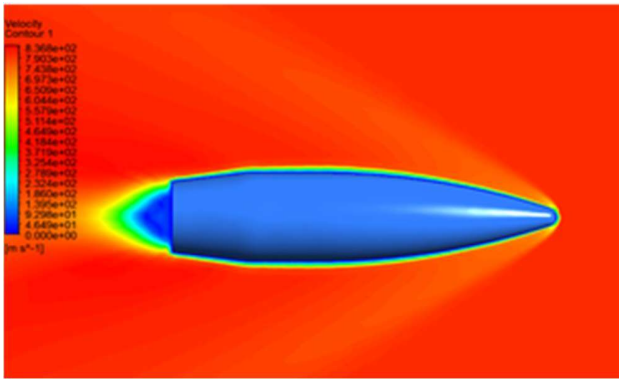


Figure 5.
Velocity analysis

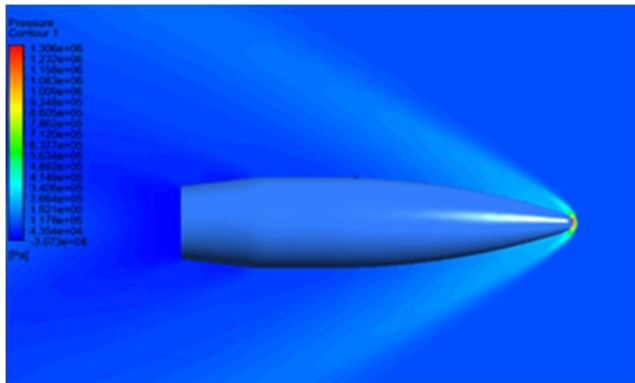
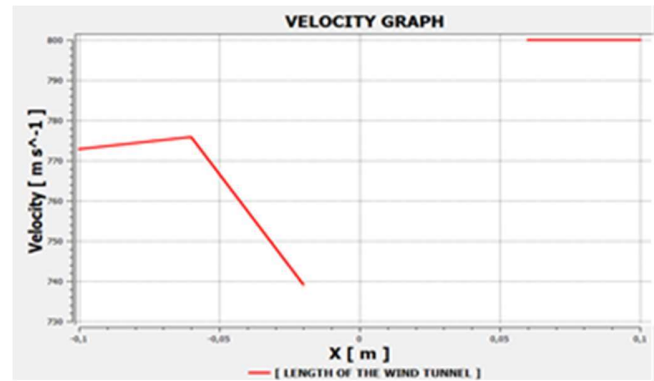
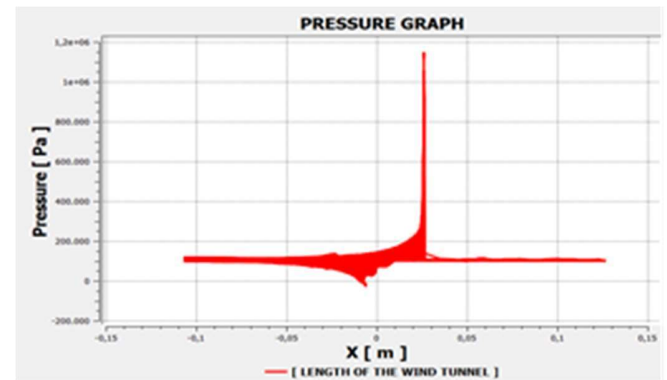


Figure 6.
Pressure analysis



Conclusions

In this study, in order to contribute to the related field, the contribution of the aerodynamic behavior of the projectile geometry to the projectile range is investigated. For this purpose, after the necessary literature review, computerized analyses were performed. The 7.62x51 mm bullet core was designed in SolidWorks and analyzed in ANSYS Fluent software.

- As a result of the analysis, it was seen that the flow velocity around the projectile, which has an exit velocity of 800 ms^{-1} , decreases to 44 ms^{-1} in the rear region of the projectile.
- When the average flow velocity around the projectile core was evaluated, it was observed that there was a decrease in the flow velocity around the core. There was a 94.5% reduction in the rear part of the bullet.
- At the tip of the projectile, the pressure increased to 1300000 Pa, while at the rear of the projectile, it dropped to -30000 Pa.

- The drop behind the bullet is calculated at 130%.

Peer-review: Externally peer-reviewed

Author contributions:

O.Yazıcı : Writing, Literature search, analysis

Ş.K: Supervision, literature search, writing manuscript, methodology

O.Yıldırım : Supervision, conceptualization

Ö. Ç: Investigation, analysis

Financial disclosure: This research received no external funding.

Conflict of Interest: The author has no conflicts of interest to declare.

References

- Bogdanović-Jovanović, J. B., Stamenković, Ž. M., & Kocić, M. M. (2012). Experimental and numerical investigation of flow around a sphere with dimples for various flow regimes. *Thermal Science*, 16(4), 1013-1026.

- Choi, J., Jeon, W. P., & Choi, H. (2006). Mechanism of drag reduction by dimples on a sphere. *Physics of Fluids*, 18(4).
- Chowdhury, H., Loganathan, B., Wang, Y., Mustary, I., & Alam, F. (2016). A study of dimple characteristics on golf ball drag. *Procedia engineering*, 147, 87-91.
- Cummings, R. M., Yang, H. T., & Oh, Y. H. (1995). Supersonic, turbulent flow computation and drag optimization for axisymmetric afterbodies. *Computers & fluids*, 24(4), 487-507.
- Doğru, M. H. (2017). Investigation of Velocity Distribution and Turbulent Energy for the Different Tip Shaped Projectiles. *Çukurova University Journal of the Faculty of Engineering and Architecture*, 32(3), 39-46.
- Hao, B., Jiang, Q., Xu, C., & Liu, L. (2024). Aerodynamic Characterization of Bullet Heads with Different Arcuate Curves. *Journal of Applied Fluid Mechanics*, 17(5), 1015-1026.
- Khan, T.H., & Saha, S. (2013). *Numerical Simulation and Aerodynamic Characteristic Analysis of a Paraboloid Tip bullet*, 4th Global Engineering, Science and Technology Conference, Bangladesh, 1–8.
- Litz, B. (2016). Aerodynamic drag modeling for ballistics part 1 aerodynamic drag 101", *Applied Ballistics*, 1: 1–13.
- Murphy, C. (1953). On Stability Criteria of the Kelley-McShane Linearized Theory of Yawing Motion, Ballistics Research Laboratories Report, USA, 853.
- Nietubicz, C. J., & Struik, W. B. (1988). *Navier-Stokes Code Verification for Projectile Configurations at a Supersonic and Transonic Velocities*, AIAA 15th Aerodynamic Testing Conference, USA.
- Salunke, S., Shinde, S., Gholap, T. B., & Sahoo, D. (2023). Comparative Computational Analysis of NATO 5.56 mm, APM2 7.62 mm and AK-47 7.82 mm Bullet Moving at Mach 2.0 in Close Vicinity to the Wall. *FME Transactions*, 51(1).
- Selimli, S. (2020). Numerical Investigation of the Effect of Surface Geometry on Projectile Aerodynamic Behavior, *Polytechnic Journal*, 299-304.